

STUDY OF VIBRATION INDUCED STRESSES IN DESIGN OF FUEL-ELEMENT  
SUPPORT ASSEMBLY FOR TUNGSTEN WATER-MODERATED  
NUCLEAR REACTOR

By Ivan B. Fiero and Donald W. Adams

Lewis Research Center  
Cleveland, Ohio

NATIONAL AERONAUTICS AND SPACE ADMINISTRATION

---

For sale by the Clearinghouse for Federal Scientific and Technical Information  
Springfield, Virginia 22151 - CFSTI price \$3.00

## ABSTRACT

The results of vibration tests on a concentric-tube fuel-element support structure for the Tungsten Water-Moderated Reactor are presented. The assembly is a composite material inner tube separated from a concentric aluminum outer tube by springs. The tests show that the assembly must be supported on both ends and at the center of the aluminum tube by the reactor structure. With a cold reactor, only one spring is necessary to ensure that the support tube will withstand lateral vibrational loads. When the reactor is hot, three springs are required. Stress distributions and parameters affecting bending vibration response are discussed.

STAR Category 32

STUDY OF VIBRATION INDUCED STRESSES IN DESIGN OF FUEL-ELEMENT  
SUPPORT ASSEMBLY FOR TUNGSTEN WATER-MODERATED  
NUCLEAR REACTOR

by Ivan B. Fiero and Donald W. Adams  
Lewis Research Center

SUMMARY

The Tungsten Water-Moderated Reactor (TWMR) for rocket propulsion application incorporates long thin-walled stainless steel-molybdenum-tungsten tubes in which the nuclear fuel elements are positioned and supported. In order to provide insulation between this hot support tube and the water moderator, an aluminum tube is positioned concentrically about the support tube with the annular space filled with stagnant gas. Thin corrugated springs are used within the annular space to ensure separation of the tubes while under lateral loads and to prevent excessive heat loss, as would be the case with solid supports between tubes. The springs can also accommodate the relative thermal expansion between the support tube and the aluminum pressure tube.

In order to check the feasibility of this design approach two models of the support tube were fabricated: (1) a model to simulate cold support-tube properties for boost vibrations and (2) a model to simulate the hot support-tube properties for flow-induced vibrations during reactor operation. Configurations of each model were tested with different numbers of corrugated springs, with and without pressure-tube lateral supports, presence or absence of water moderator, and variations in amplitude of the input forcing function.

The tests of both models indicate that the design is feasible from the standpoint of resonant bending stresses. The test results indicate that the cold tungsten tube is rigid enough that only one spring is necessary to prevent excessive lateral displacement and stress. The less rigid hot model required three springs.

The addition of pressure-tube lateral supports decreases the unsupported span and, consequently, decreases the stresses. Because a spring is located relatively near the lateral support location, the support tube also responds as though it had a simple support at midspan. The effect of the corrugated springs is to couple the support tube and pressure tube together.

Water surrounding the pressure tube had several effects on the lateral displacement: (1) buoyancy decreased the displacement, (2) hydraulic drag tended to decrease the displacement, and (3) the virtual mass of the water tended to increase the displacement.

## INTRODUCTION

The Tungsten Water-Moderated Nuclear Rocket (TWMR) (ref. 1) is a system which could be used as an upper stage engine in a long space mission where high specific impulse is necessary. Because it is an upper stage, the reactor must be capable of withstanding boost vibrations as well as normal flow induced vibrations associated with its own operation.

The booster-induced lateral vibrations are expected to be random forcing frequencies between approximately 5 and 2000 hertz and have an amplitude of about 1 g and probably not exceeding 2 g's. The reactor is essentially at ambient temperature during boost; therefore, the refractory metal tungsten must withstand vibration in a relatively brittle condition. During reactor operation, the flow of the hydrogen propellant and water moderator through the reactor is a potential source of vibration. Because of the high operating temperature of the reactor, the refractory materials will lose a considerable amount of rigidity which might result in large displacements and stresses.

The most critical member within the reactor of the TWMR is the fuel-element support tube (ref. 1). This tube serves three major functions: (1) it supports and positions the fuel elements, (2) it serves as a propellant flow passage, and (3) it functions as the inner wall of a stagnant gas gap for thermal insulation between the fuel and water moderator.

A schematic of the fuel-element support structure for the TWMR is shown in figure 1. The support structure consists of the long thin-walled stainless-steel-molybdenum-tungsten support tube inside of a thin-walled aluminum pressure tube. Because of the

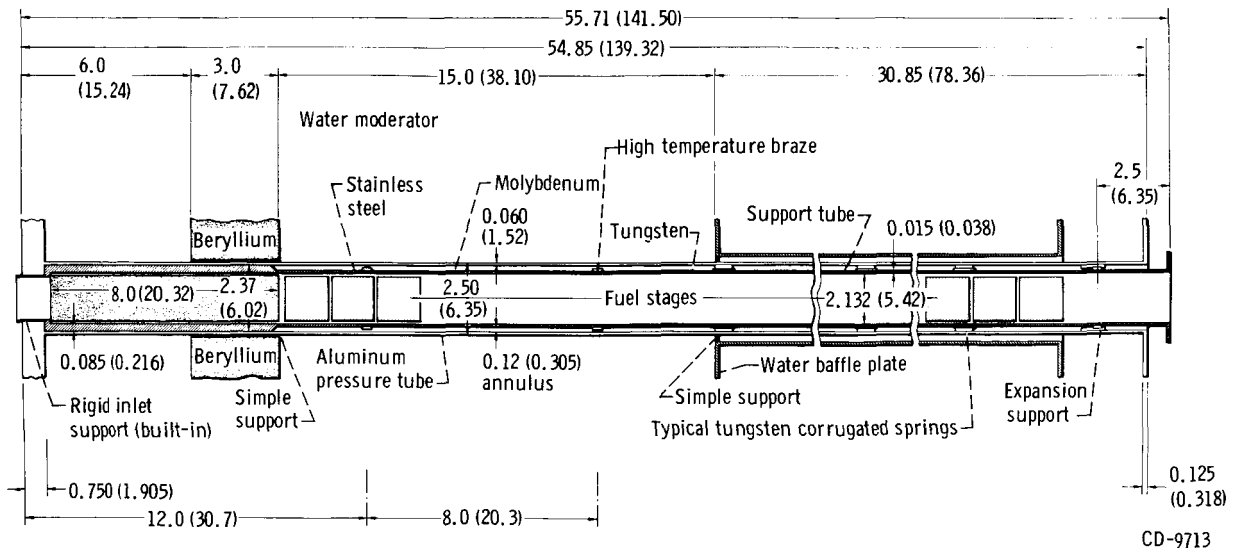


Figure 1. - Fuel-element support structure of tungsten water-moderated reactor. (All dimensions are in inches (cm).)

relative thicknesses of the inlet and exit headers, the inlet end of the pressure tube is essentially a fixed (build-in) support, while the exit end is approximately simply supported. The pressure tube is also simply supported near the center by a water baffle plate. Another simple support is also possible at the beryllium reflector, if necessary. The inlet end of the composite support tube is approximately a fixed support. However, the exit end, which is held in place with four radial splines, is a simple support. This type of spline support is necessary to accommodate radial and axial thermal expansion of the support tube during operation. Corrugated springs in the annular gas gap between tubes prevent the support tube from impacting the pressure tube while under lateral vibration.

The support-tube vibration problem was studied analytically using both analog (ref. 2) and digital (ref. 3) techniques. An inability to develop an accurate mathematical model of damping reduced the validity of the study in the vicinity of the resonant frequencies. In order to establish confidence in the support-tube design, an experimental investigation of the response of the tube to lateral bending vibrations was undertaken. A study of the tube response would yield information on the bending stress distribution at the resonant frequency to determine whether the tube would fail and information on the effect of the number of springs, the additional simple supports on the pressure tube (from the water baffle plate and beryllium reflector), and the water moderator.

Two different models of the support tube were fabricated for study because drastically different temperature distributions in the support tube are associated with each of the two sources of excitation: (1) booster vibration from a lower stage and (2) moderator and propellant flow induced vibration during reactor operation. The first model simulated the geometry and properties of the cold (ambient temperature) support tube as it would be for boost phases. This model was essentially identical to that of the TWMR design in both geometry and materials. The second model had nearly the same geometry but was constructed of different materials which, at room (or ambient) temperature, simulated the dynamic characteristics of the TWMR tube at the higher temperatures associated with full-power operation.

Only lateral input vibration was considered. However, the amplitude of the input was varied up to as high as 3 g's for the tube design with the lateral supports, springs, and water moderator as it would appear in the TWMR.

## DESCRIPTION OF TEST MODELS, EQUIPMENT, AND INSTRUMENTATION

### Model Description

Cold vibration model. - During chemical booster operation of the other stages of the vehicle of which the TWMR would be a part, the TWMR is expected to be subjected to

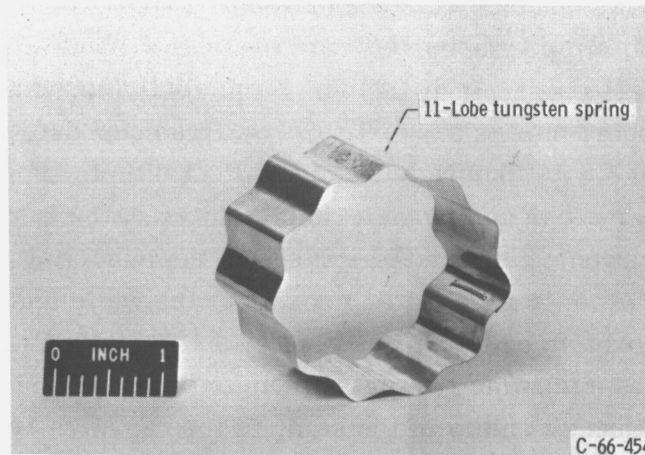


Figure 2. - Typical corrugated spring.

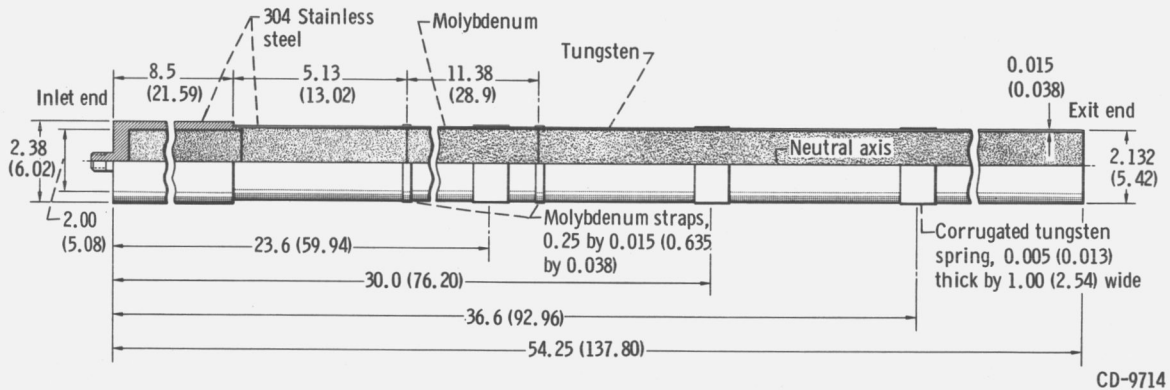


Figure 3. - Cold support-tube vibration model. (All dimensions are in inches (cm).)

booster-induced lateral vibrations with a random forcing frequency between 5 and 2000 hertz. For all practical purposes, the reactor is at ambient temperature during the boost phase. Thus, the model must simulate the properties of the fuel-element support tube at ambient temperature.

The cold vibration model was fabricated essentially identical to the specifications of the TWMR support-tube design in material, geometry, and weight, but with some minor modifications for the joint braze and for the fuel-element supports. Rather than high-temperature braze or welding, all support-tube joints were silver soldered. Reinforcing straps 0.015-inch (0.038-cm) thick were utilized for added strength. These straps provided local reinforcement only and had negligible effect of the overall tube behavior. It was decided to employ one pin support per fuel element and to mount this pin in a set of holes on the neutral bending axis of the support tube. This arrangement avoids possible

large stress concentrations around the pin holes because the only stresses present on the neutral axis will be the pin bearing stress. Any pin bearing holes in the TWMR design were locally reinforced to eliminate the high stress concentration. A preliminary vibration test of the fuel element indicated that it was structurally sound and had a rigid body behavior with respect to the support tube. Therefore, 26 solid dummy weights (0.86 lb (0.390 kg) each) replaced the actual fuel elements.

Rather than machine a beryllium plug for the inlet end of the tube, the wall thickness of the first stainless-steel-tube section was increased to 0.2 inch (0.5 cm) to simulate the weight effect of the plug. The additional rigidity is negligible because the inlet end has built-in characteristics.

Three 1.00-inch (2.54-cm) wide corrugated tungsten springs (shown in fig. 2) were located in the axial positions as shown in figure 3. These springs are fabricated from 0.005 inch (0.013-cm) thick sheet stamped into 11 corrugations and formed into a cylindrical shape by stapling the ends together.

The geometry and materials used for the support-tube model are also shown in figure 3.

The aluminum pressure tube is identical to that of the TWMR design.

For the tests on the cold model, the lateral supports from the water baffle plate and the beryllium reflector were not used.

Hot vibration model. - During reactor operation the flow of the hydrogen propellant and water moderator are potential sources of mechanical vibration. The high operating temperature of the support tube results in a decrease in the elastic modulus and, consequently, a loss in rigidity of the tube. Because of the problems associated with a vibration test at the operating temperature, the model must simulate the high-temperature properties of the support tube at room temperature.

In order to develop an accurate model, the axial temperature distribution (fig. 4) and the associated elastic modulus (fig. 5) were first determined. Then, using appropriate geometry parameters, the support-tube flexural rigidity was calculated as a function of axial position. Figure 6 shows a comparison between the flexural rigidity for the model at room temperature and the actual support tube at operating temperature. In addition, other modeling parameters include the tube mass distribution and end constraints. Appendix A contains a detailed description of the modeling theory. The strains in the model multiplied by the local modulus of elasticity of the actual support tube at operating temperature yields the operating stresses as shown in appendix A. The geometry and materials used in the model are summarized in figure 7.

The five tube sections were joined by shrinking on a 0.25-inch (0.635-cm) wide by 0.015-inch (0.038-cm) thick stainless-steel band at each butt joint. All joints were then furnace copper brazed at 2000<sup>o</sup> F (1095<sup>o</sup> C). Dummy weights were used to simulate the fuel elements as had been done with the cold model. Corrugated molybdenum springs

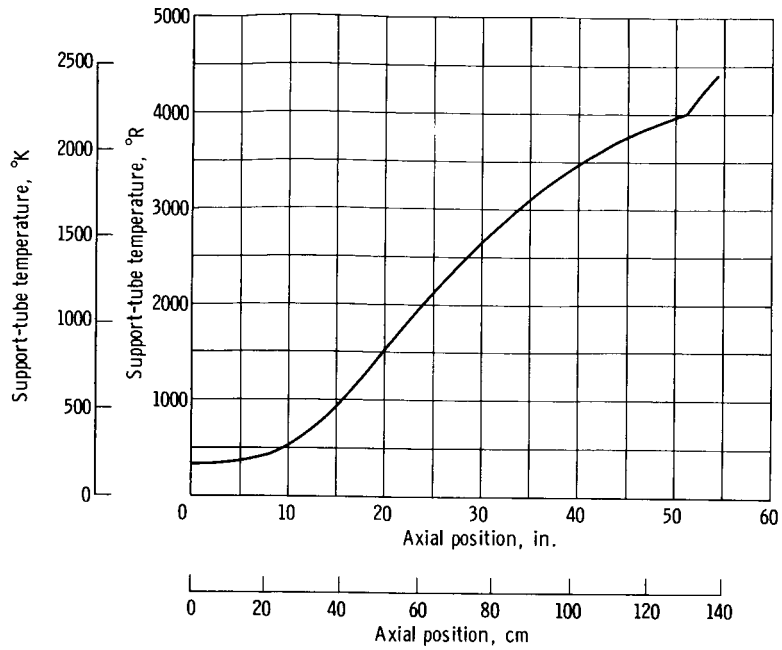


Figure 4. - Support-tube temperature distribution (from ref. 1).

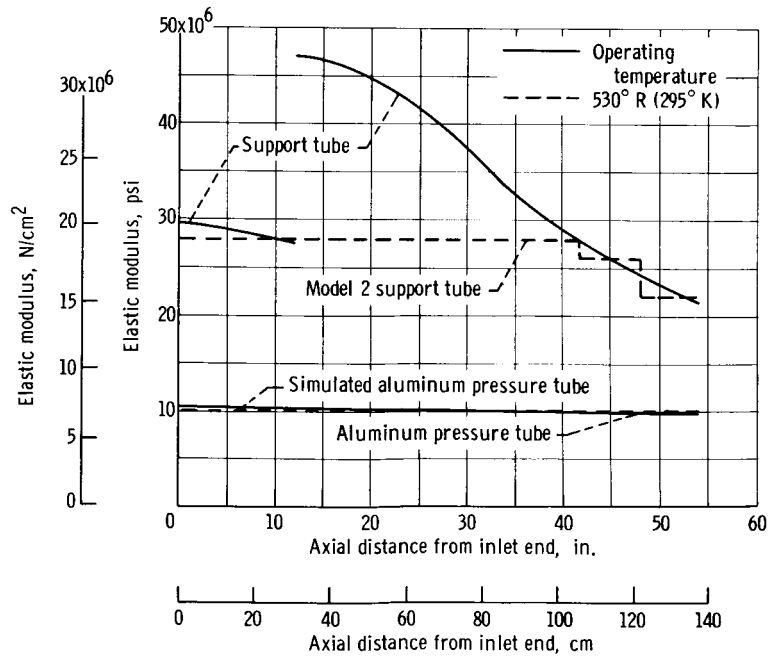


Figure 5. - Support-tube and aluminum pressure tube elastic moduli. Basic modulus as function of temperature data were taken from references 4 to 6 and 13.

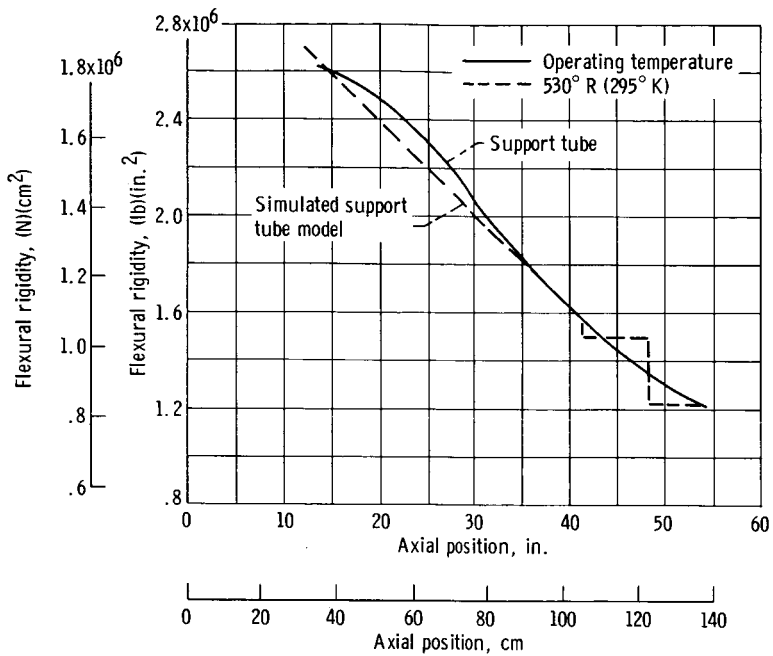
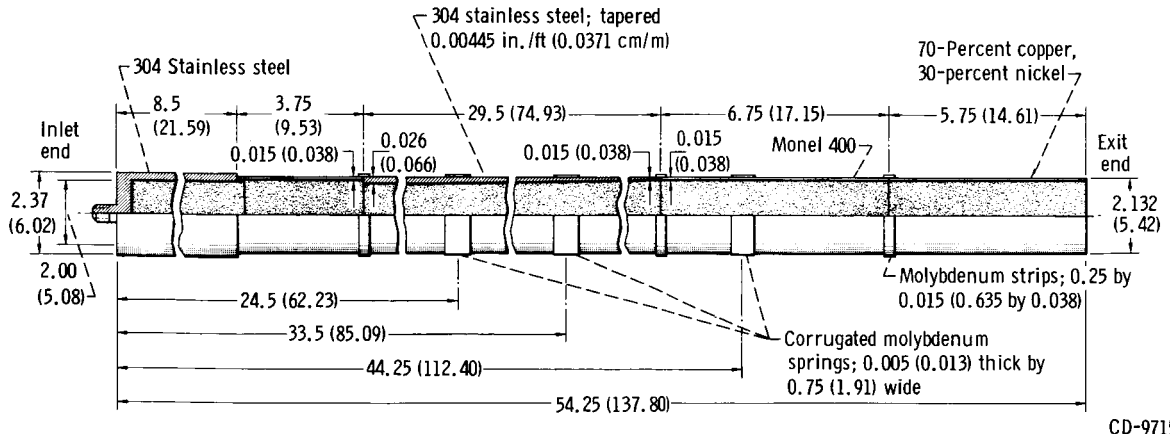


Figure 6. - Support-tube flexural rigidity.



CD-9715

Figure 7. - Hot support-tube vibration model. (All dimensions are in inches (cm) unless otherwise noted.)

0.75-inch (1.91-cm) wide by 0.005-inch (0.013-cm) thick were located at three axial positions as shown on the schematic of the hot model (fig. 7). These molybdenum springs simulate the elastic properties of the hot tungsten. The springs were also located further apart and nearer the hot exit end in this model because of experimental results obtained from the cold vibration model. These springs contained 12 corrugations rather than 11, but this will have a very negligible effect on the spring constant.

The aluminum pressure tube is the same one used with the cold support-tube model.

A lateral support for the aluminum pressure tube was located near the position of the inlet end reflector and another located at approximately midspan to simulate the water baffle plate. Although both supports are effectively simple supports, the bearing surface of the reflector support is twice that of the baffle plate. Also, the supports for the model are not circumferentially continuous, but are in three approximately  $68^\circ$  strips around the periphery. This was as large as practicable and still enabled strain-gage leads to be placed along the outer surface of the tube.

### Test Fixture and Support Arrangement

The vibration test holding fixture (shown in fig. 8) was fabricated from structural aluminum components. Wooden blocks were added between the fixture webs to increase

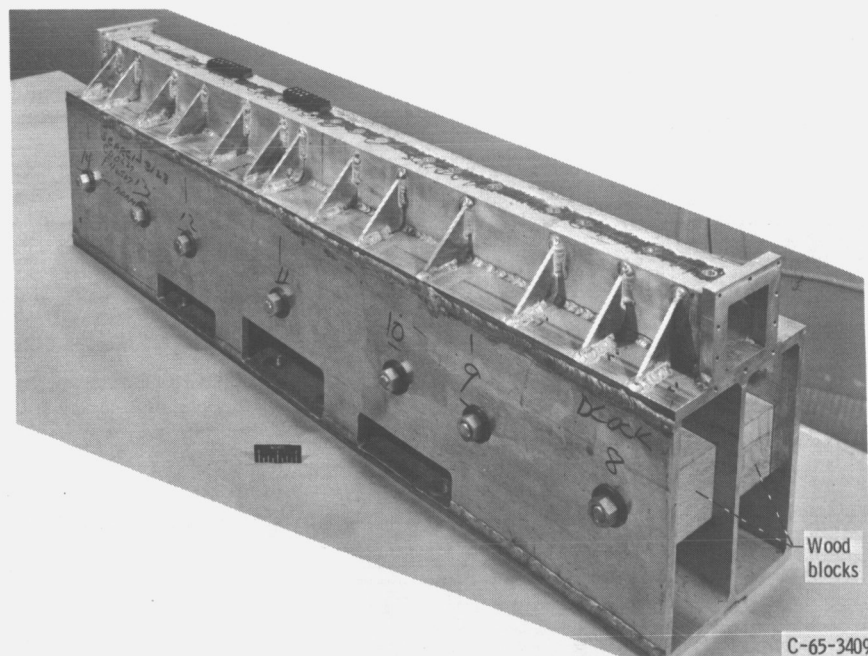


Figure 8. - Aluminum support fixture.

lateral and torsional stability. The fixture was bolted to a 28 000-pound-force (125 000-N) rated, electrodynamic vibration exciter. Vibration tests indicated a first-mode resonance of the fixture at approximately 500 hertz, much higher than the fundamental frequencies of the pressure-tube - support-tube configurations. The volume of water within the fixture after the pressure tube is inserted is approximately 0.1 cubic foot (2800 cm<sup>3</sup>), which is equivalent to the amount of water surrounding each individual tube in the TWMR.

The fixture shown in figure 8 was later modified to incorporate the pressure tube lateral supports used for tests on the hot model. These lateral supports (shown in fig. 9) are simply small plates inserted through slots in the sides of the fixture and held in position with bolts. The ends with circular arcs are in contact with the surface of the aluminum pressure tube.

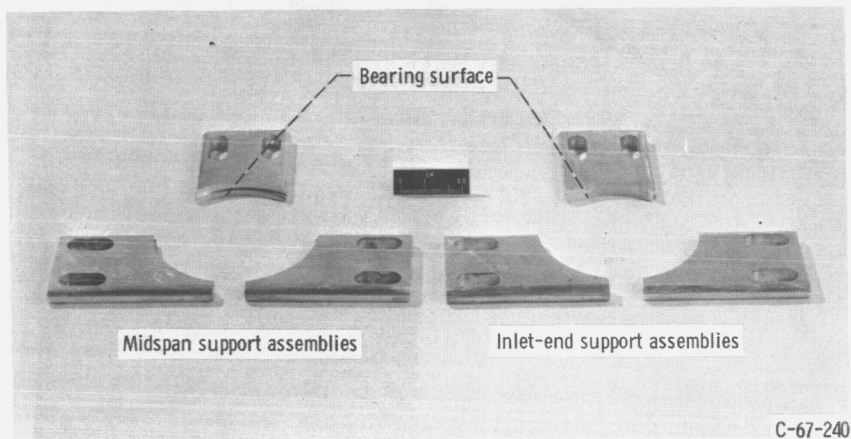
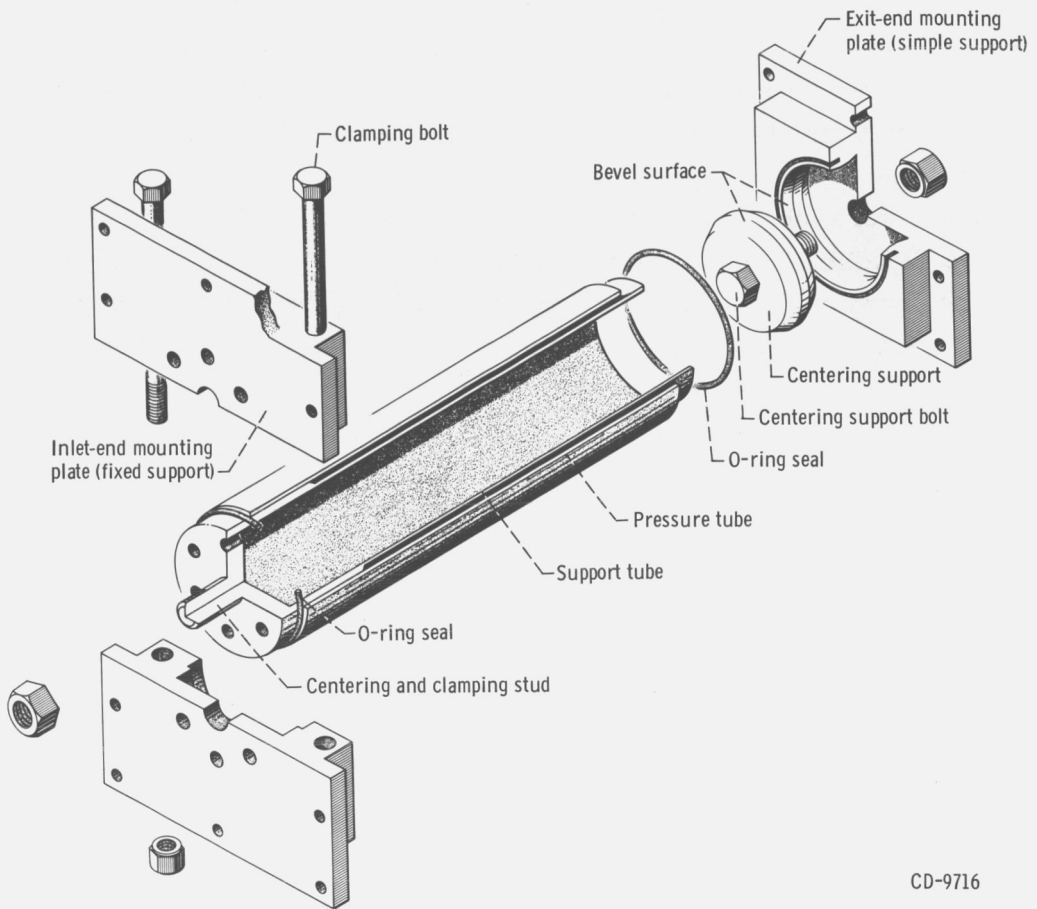


Figure 9. - Pressure-tube lateral supports.

End mounting plates are used to support the tubes inside the fixture and provide a water-tight seal when the fixture is filled with water. These plates provide the approximate clamped-simple support arrangement for both the pressure and support tubes. A schematic of the end plates is shown in figure 10. Both plates consist of two pieces: the inlet end plate is split into halves, and the exit end consists of the plate and a support-tube centering support. The build-in support for both the pressure tube and support tube is provided by clamping the halves of the inlet plate together onto the tubes. In addition, the support tube is securely fastened with a stud through the end as shown in the figure. When the mounting plate is fastened to the fixture, the inlet ends of the tubes are essentially fixed. The simple support of the exit end of the support tube is provided by the beveled surfaces of the plate and centering support. The pressure tube also has a sliding fit in the exit plate which will give a simple support. Both ends of the pressure tube are sealed with rubber O-rings.



CD-9716

Figure 10. - Support arrangement of fixture mounting plates.

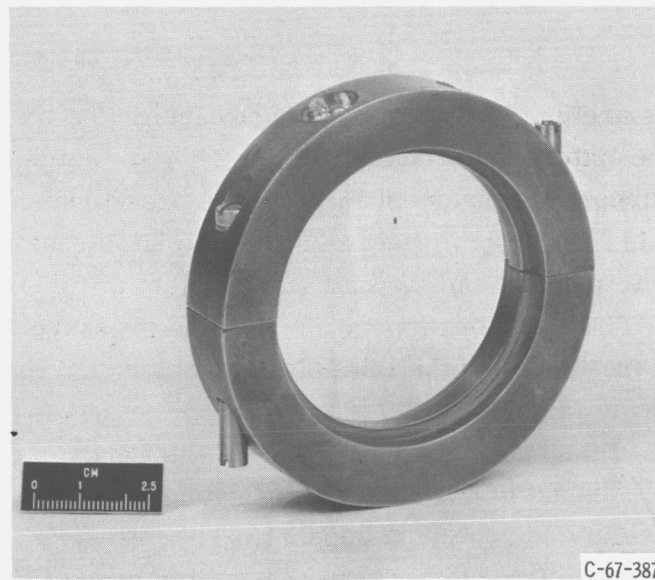


Figure 11. - Split copper weight for simulating water virtual mass.

Alternate backing plates were provided in order to mount the tubes on the outside of the fixture. The purpose of this was to enable copper weights (fig. 11) to be fastened to the pressure tube to simulate the effective mass of the water. The derivation for the effective mass of the water using the mass of the copper weights is given in appendix B.

## Model Variations

Several variations involving different numbers of corrugated springs, pressure-tube lateral supports, and presence or absence of water for both the cold and hot models were tested.

For the cold vibration model, a test was performed on the support tube alone, and then on the tube-assembly configuration (both tubes together). The assembled configuration was tested with and without the presence of the water moderator, each with zero to three corrugated springs in position. All these tests were frequency sweeps at approximately 1-g level.

As was the case for the cold model, the hot model was tested as an individual tube. The aluminum tube was also tested by itself. In addition, the aluminum tube was tested singly in a water environment, and both with and without lateral supports at midspan. The effect of the displaced water mass was investigated by vibrating the aluminum tube with copper weights spaced along the axis. The assembled pressure and support tubes were tested with one to three springs in position, with and without a water environment and with and without lateral supports. An additional variation was without a lateral support near the inlet end but with the midspan support in position. Most of the cases were with 1-g input lateral load; however, the configuration that appeared to be the most promising candidate for the final design was also vibrated with an input lateral load of 2 and 3 g's.

The natural frequency of the various assemblies was found by a sweep from 5 to 2000 hertz, and then the amplitude response was found by conducting constant-frequency tests at several incremental frequencies spanning the resonance. For the cold model, only sweeps through the frequency band were performed.

## Instrumentation

Both the support tube and the pressure tube were instrumented with strain gages; this enabled a direct determination of the bending stress distribution in both tubes. The strain-gage leads could not be located in the annular gap between tubes because of the corrugated springs and also because the relative displacement between tubes would be se-

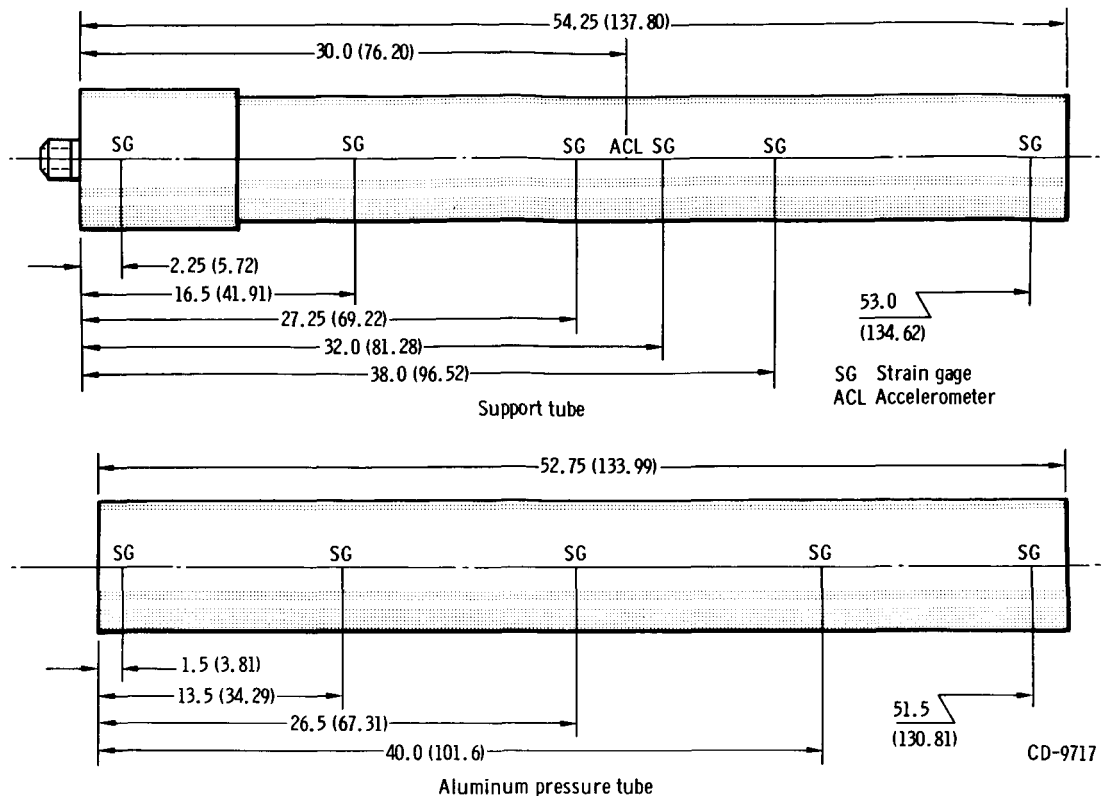


Figure 12. - Location of instrumentation for cold support-tube model and aluminum pressure tube. (All dimensions are in inches (cm).)

verely affected by the leads. Consequently, the support-tube leads were placed inside the support tube and the pressure-tube leads were placed on the outer surface of the pressure tube. The position of the strain-gage leads not only required the compromise of the continuous lateral supports mentioned previously, but also they had a small but undetermined effect on the drag of the tube in the water. In addition to the bending stress distribution, acceleration data were required in some tests; therefore, miniature piezoelectric accelerometers were employed. These accelerometers were installed in the simulated fuel elements. The strain-gage and accelerometer data were used to determine the natural frequency, strain magnitude, and phase relations.

Figure 12 shows the location of the strain gages and accelerometers on the cold vibration model. The gages were located on the maximum bending fiber of the tubes at various axial locations. At each location, four strain gages formed a four-arm active Wheatstone bridge. The bridge output voltages were amplified by high-gain amplifiers and fed into an oscillograph recorder with optical galvanometers, producing a photographic record of the strains. A time-mark generator within the oscillograph allowed strain as a function of frequency to be determined. All components had a flat frequency response over a 2-kilohertz frequency band. The oscillograph records were resolvable to about

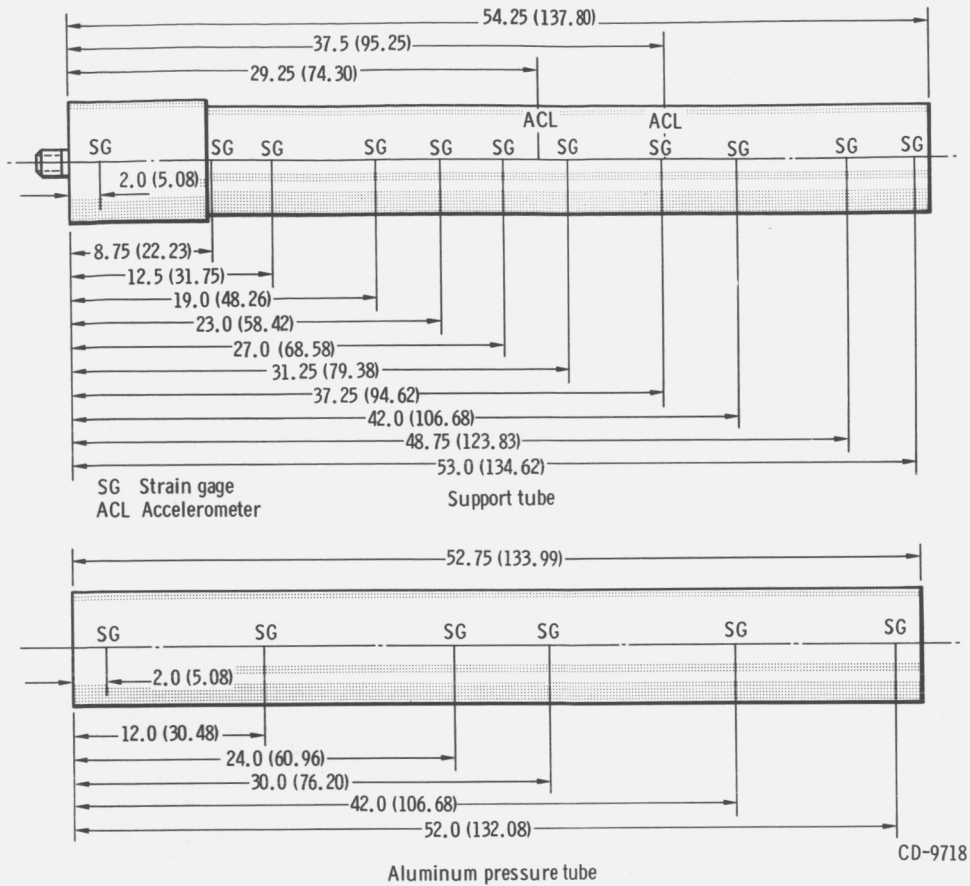


Figure 13. - Location of instrumentation for hot support-tube model and aluminum pressure tube. (All dimensions are in inches (cm).)

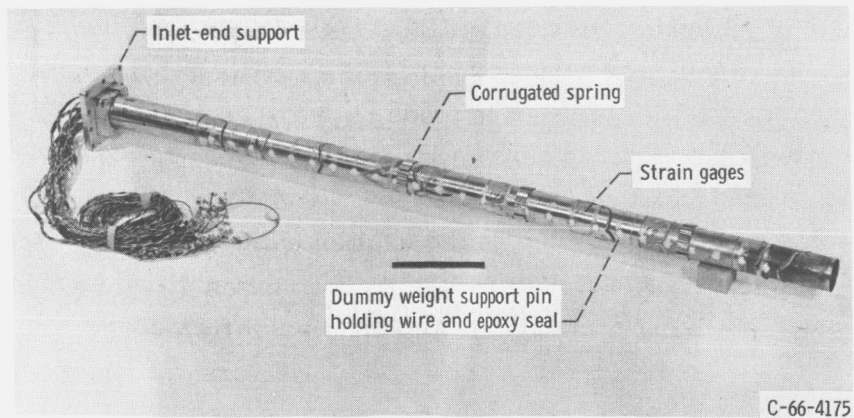


Figure 14. - Instrumented hot support-tube model.

$\pm 100$  psi ( $69 \text{ N/cm}^2$ ) in addition to an instrumentation error of  $\pm 4$  percent, which was well within the limits of interest.

Figure 13 shows the locations of the strain gages and accelerometers on the hot vibration model. Because the lateral supports to the pressure tube were used on this model, the stress pattern would be more complex, consequently more strain gages were used. Figure 14 is a photograph of the instrumented support tube with the inlet end-support plate in position. The instrumented pressure tube is shown in figure 15.

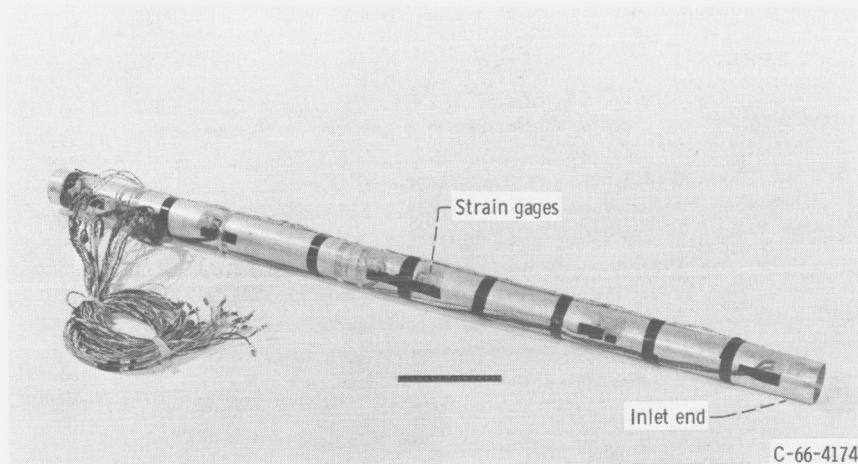


Figure 15. - Instrumented aluminum pressure tube for hot model.

The vibration exciter table was operated in two different modes. In a searching mode, the frequency sweep was from 5 to 2000 hertz at the rate of 2 octaves per minute.

Above a value of 10 hertz, the acceleration was automatically controlled to approximately 1 g. In most cases, after the resonance of a particular assembly had been determined by a frequency sweep in the search mode, a more detailed investigation of the resonance range was performed under constant-frequency manual control.

The vibration exciter control has an automatic gain control circuit which operates from an accelerometer sensor located on the exciter table to provide a feedback signal to maintain the desired g level at the exciter table. The automatic gain-control circuit has a variable time constant (or time lag) which determines the rate with which a sudden

change at the exciter table is regulated back to normal. The following table gives these time lags relative to the operating frequency:

Frequency range, Hz	Time lag, sec/dB
5 to 30	0.1
30 to 100	.03
100 to 300	.01
300 to 1000	.003
1000 and above	.001

Normally the accelerometer sensor is mounted on the exciter table. but in these experiments better control of the g level was obtained with the accelerometer mounted on the test fixture. Typical examples of the fixture response to the fixture control signal are shown in figure 16. The left curve is for a model (the single, bare support tube) in

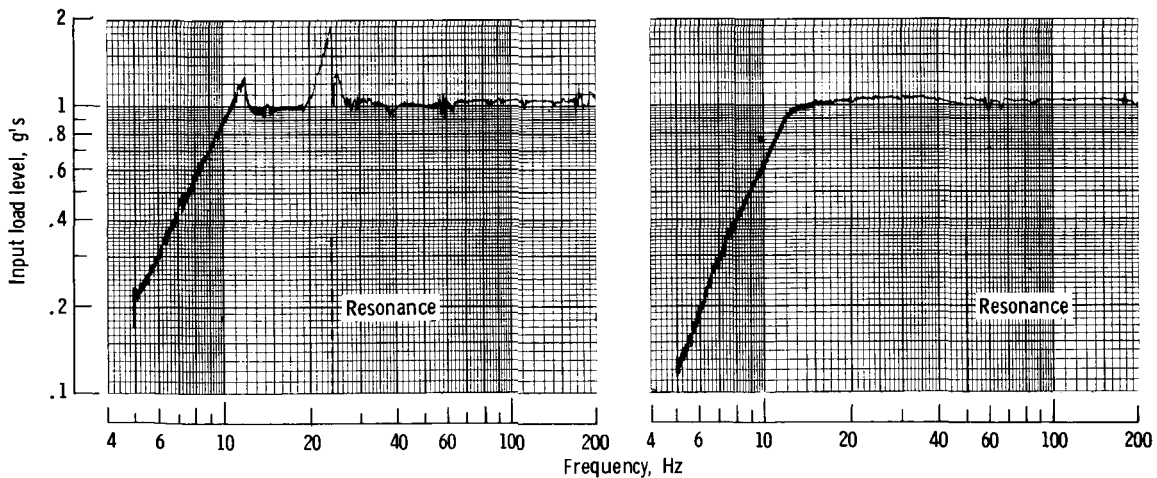


Figure 16. - Table response.

which the resonances are so sharp that, with the time lags previously quoted, the acceleration cannot be accurately regulated to 1 g automatically. The right curve is for a composite model (the complete assembly) in which the resonances are sufficiently broad to be regulated to 1 g.

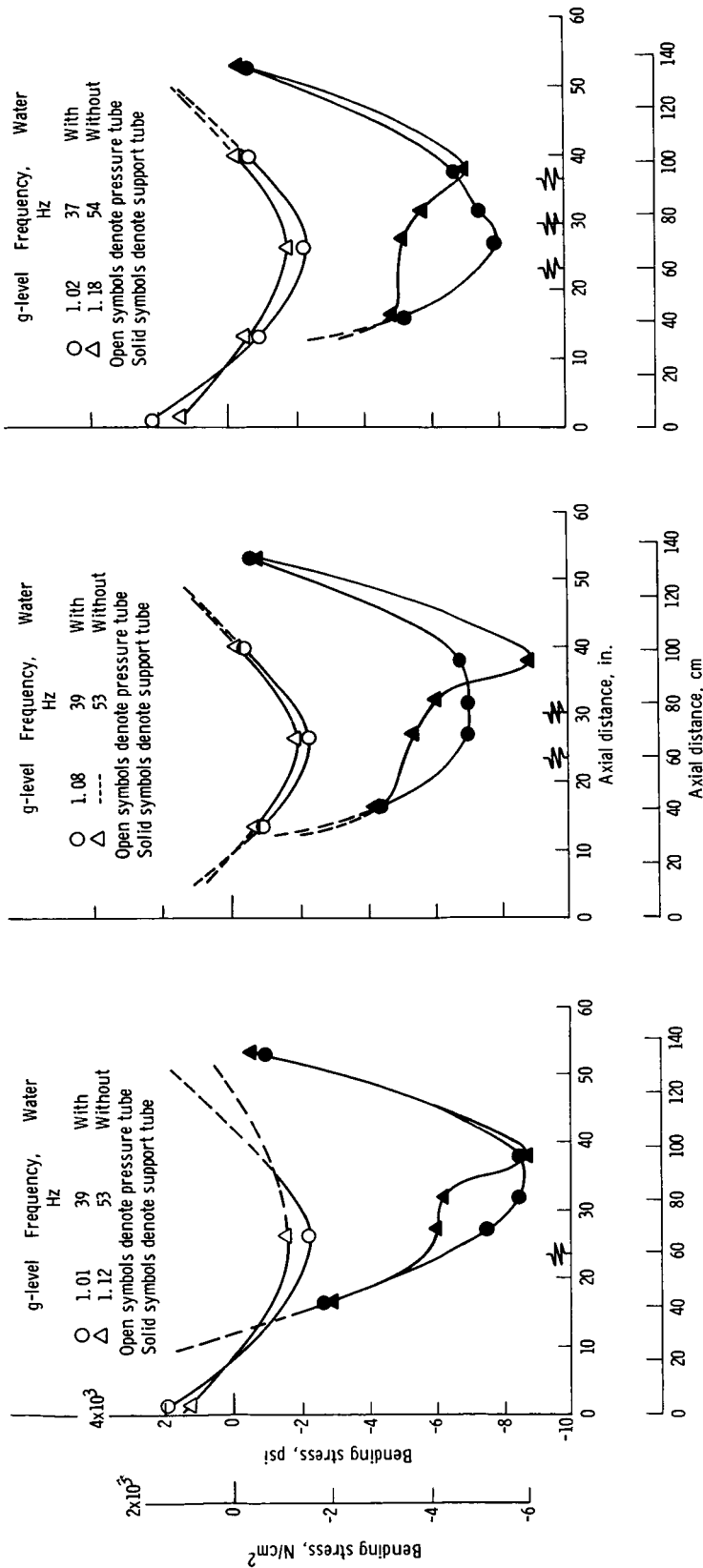
## DISCUSSION OF TEST RESULTS

The stress distributions in all the configurations tested are plotted in figures 17 to 25. The elastic modulus used for calculation of the stresses in the hot support-tube assembly is shown in figure 5 as a function of axial position. The elastic moduli of the stainless steel, molybdenum, and tungsten sections in the cold-tube assembly are given in references 4 to 6.

### Feasibility of TWMR Support Tube

The concentric design of the TWMR fuel support tube and pressure tube requires that some support, such as corrugated springs, be provided in the annulus between the tubes. Thermal growth and excessive heat transfer to the aluminum pressure tube prevent the use of thick rigid supports. A corrugated spring can provide the necessary rigidity and also keep heat loss to a minimum. Because the support tube is more rigid at room temperature, it is possible to use fewer springs than on the hot support tube. The springs can be designed such that they come into contact only when the tube thermally expands. This is important because springs located on the extremely hot portion of the tube could create excessive compressive loading if they were already in contact at ambient temperature conditions.

The vibration test data support such a corrugated spring design. Three springs located on the outlet end of the tube are sufficient to prevent excessive displacement and stress of the tube while it is hot. The test data also indicate that a single, centrally located spring would be sufficient for the cold support tube. Consequently, the two springs closest to the outlet end need not come into contact until the support tube expands. As can be seen from figure 17(a), the maximum stress for the cold model with only one spring (and without water) is 8760 psi ( $6040 \text{ N/cm}^2$ ), well within the yield stress for tungsten (ref. 4). It is assumed that the yield stress is satisfactory design criterion at the re-

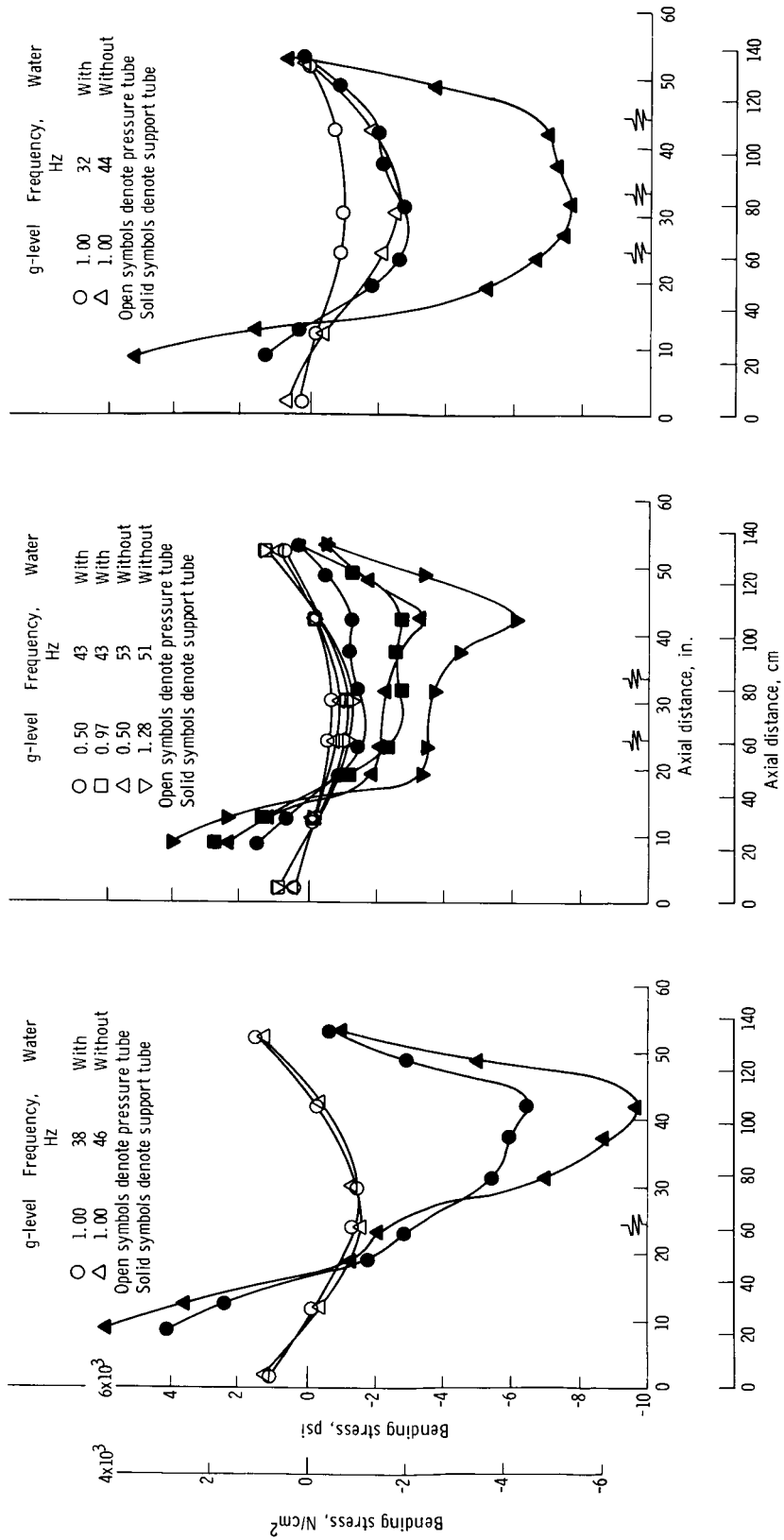


(a) Single spring.

(b) Two springs.

(c) Three springs.

Figure 17. - Bending stress in support assembly at ambient temperature.

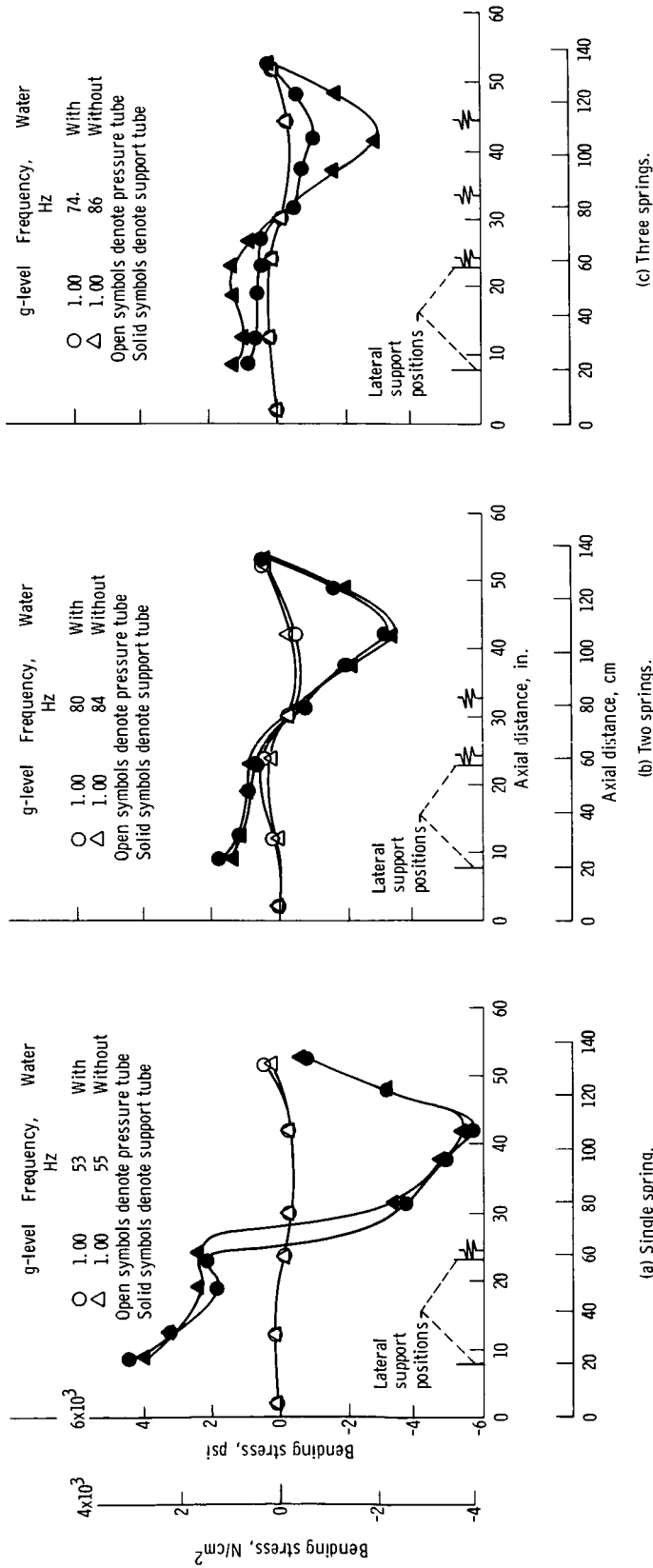


(a) Single spring.

(b) Two springs.

(c) Three springs.

Figure 18. - Bending stress in support assembly at operating temperature.



(a) Single spring.

(b) Two springs.

(c) Three springs.

Figure 19. - Bending stress in support assembly at operating temperature with lateral supports on pressure tube.

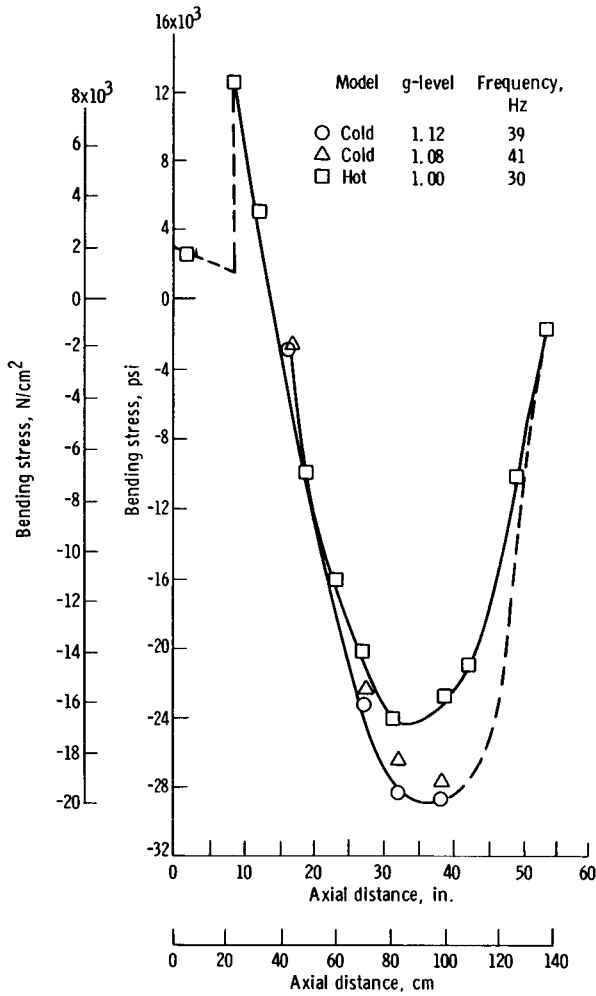


Figure 20. - Support-tube stress distribution.

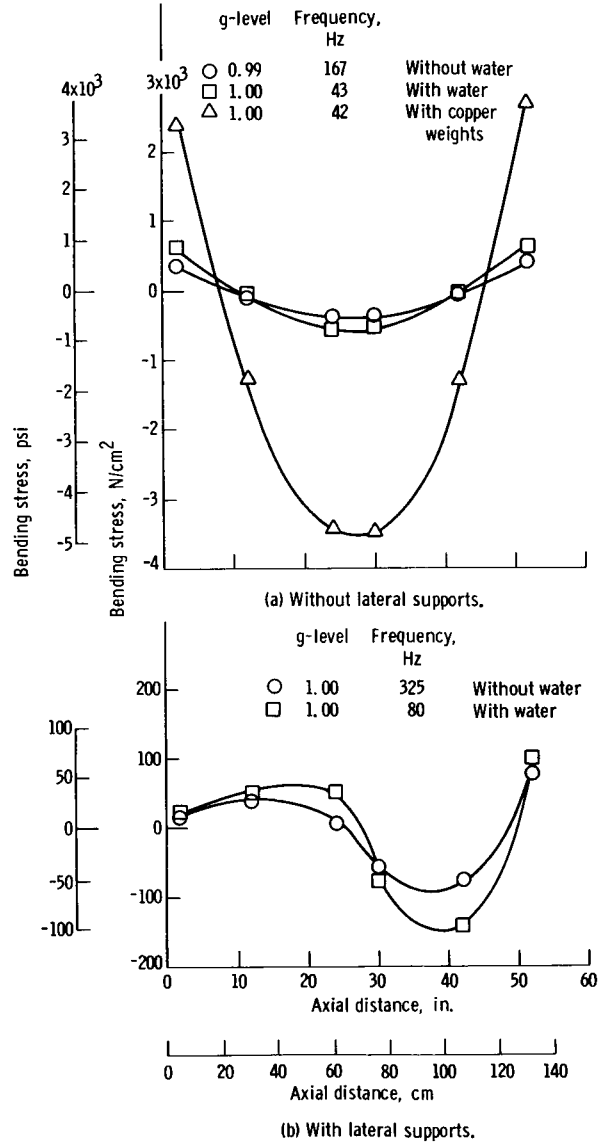


Figure 21. - Effect of water on aluminum pressure tube stress and natural frequency.

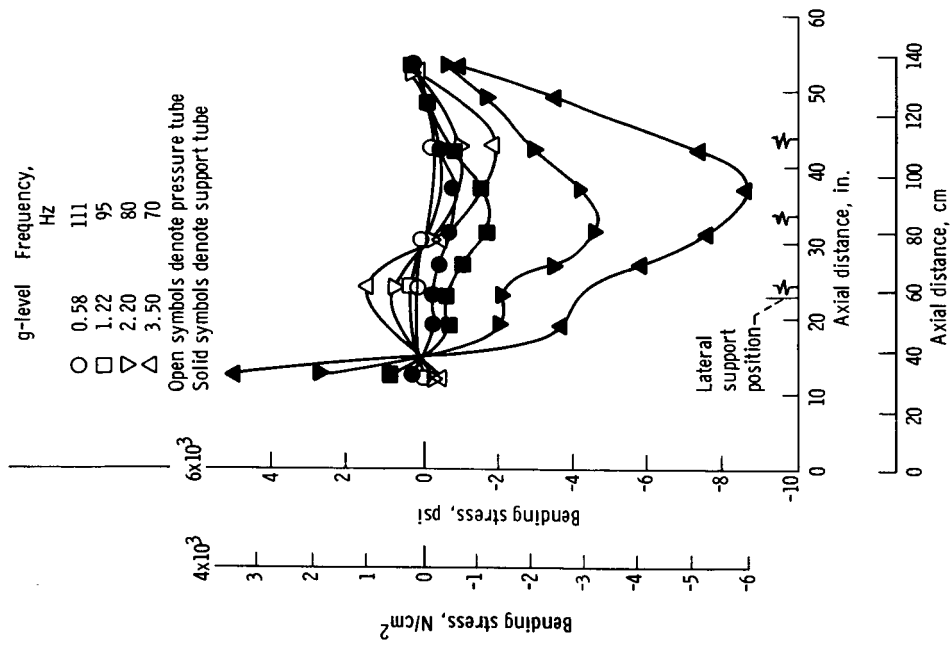


Figure 22. - Bending stress in support assembly at operating temperature with single lateral support and spring.

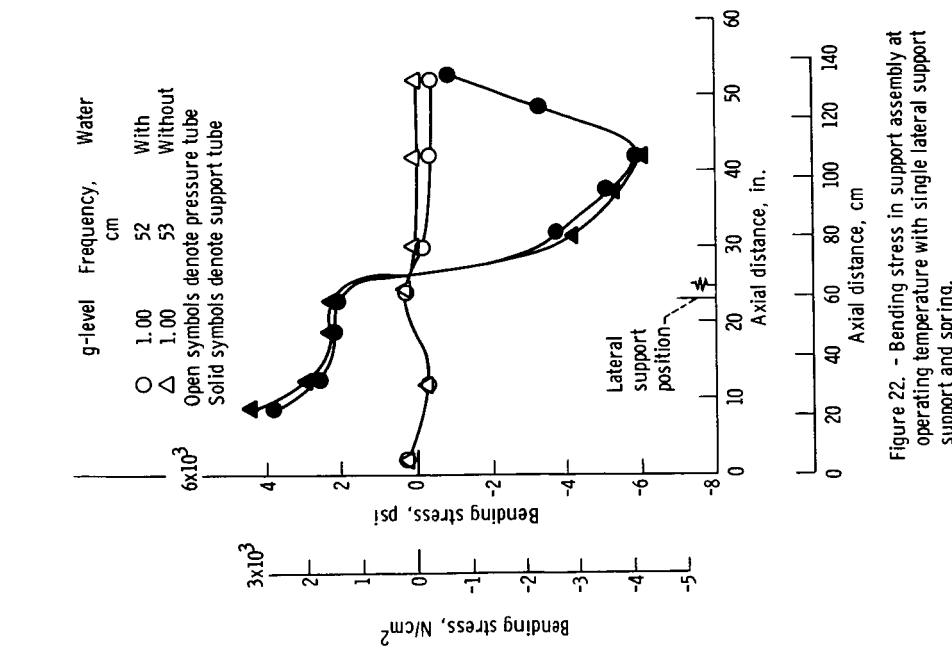


Figure 23. - Effect of input g-level on dry support assembly stress and natural frequency.

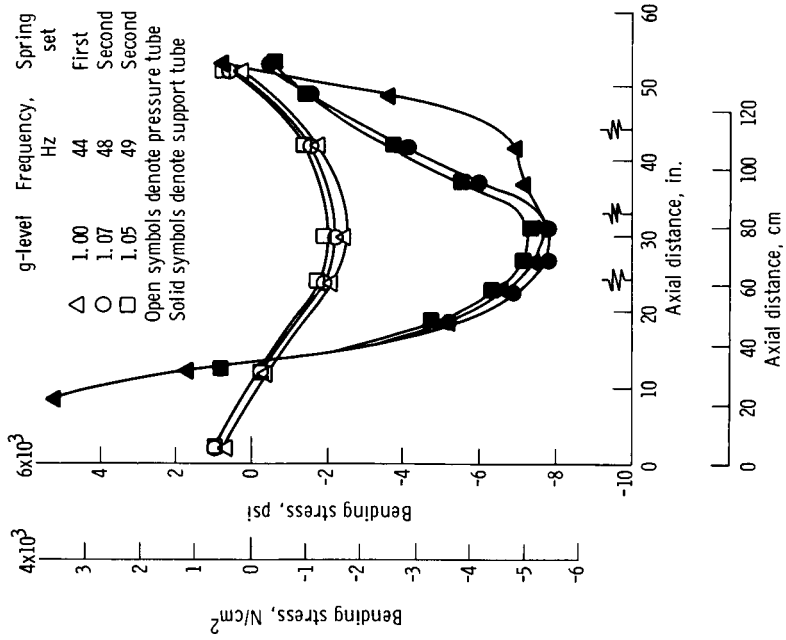


Figure 25. - Comparison of two sets of springs used in dry tests.

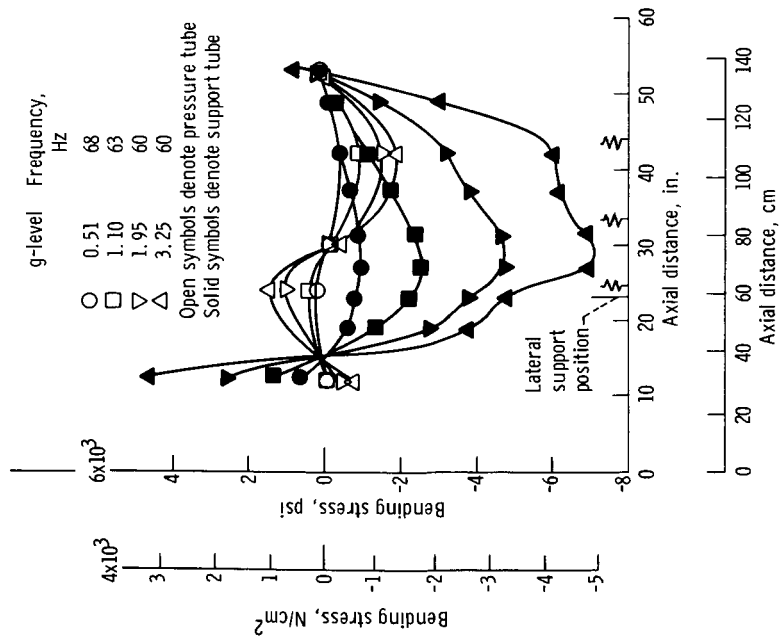


Figure 24. - Effect of input g-level on wet support assembly stress and natural frequency.

quired operating conditions. Stress with water present is approximately the same as that without water. This test was conducted without the aluminum pressure tube lateral support that was added for the hot model vibration tests. The midspan support would further reduce the stresses and displacement.

The maximum stress for the hot support tube is 9640 psi ( $6650 \text{ N/cm}^2$ ) (fig. 18(a)) for the single spring configuration. The yield stress at this point (as shown in fig. 26) indicates that this configuration would fail. The increase in stress for the hot model is due to the lack of rigidity of the tube while it is hot.

The use of additional springs in the hotter regions of the support tube reduced stresses down to levels which appear acceptable, depending on the degree of end fixity and the presence or absence of water (figs. 18(b) and (c)). Two lateral supports (at the inlet reflector location and the baffle plate) on the pressure tube plus the added springs eliminated this dependency (figs. 19(b) and (c)). Figure 19(c), with three springs, indicated a maximum stress of 2900 psi ( $2000 \text{ N/cm}^2$ ) without water and 1100 psi ( $760 \text{ N/cm}^2$ )

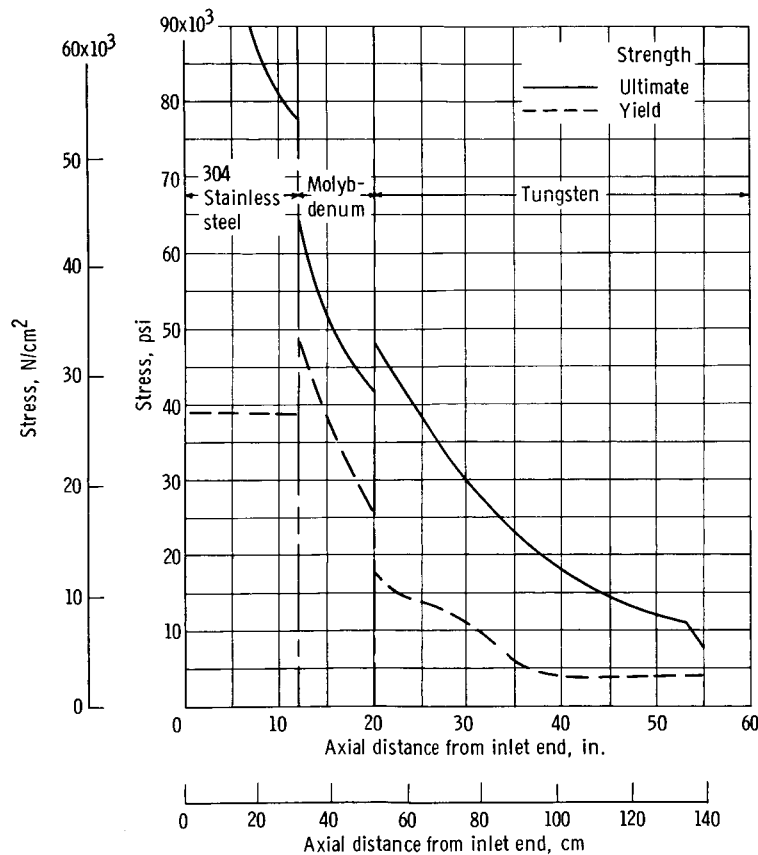


Figure 26. - Support-tube ultimate and yield strength at operating temperature. (Basic ultimate and yield strength data were taken from refs. 4 to 6.)

with water, respectively. These tests would indicate that such a design offers enough stress margin to be considered a feasible design for the assumed operational requirements.

## Effects of Various Parameters on Tube Bending Vibration Response

The tests conducted to establish the feasibility of the TWMR support tube design for both boost and hot operating conditions covered a range of structural parameters which have an effect on fuel assembly vibration response. An examination of the results of some of these tests was made in an attempt to obtain a better understanding of the effects and interrelations of these parameters. Such additional conclusions from the test results are limited by the inability to adequately control such variables as spring tightness, spring constant, and mounting end conditions for some of the tests.

Comparison of cold and hot support tubes. - The cold support tube by itself has a fundamental resonance frequency of about 40 hertz. The stresses in the cold support tube can be determined approximately from cases tested with no springs between tubes for the assembly configuration; this stress should be reasonably close to the actual stress. The tubes should not have affected each other except for the sliding fit at the entrance end, which would act slightly to stiffen the tubes and lessen the stresses. These configurations indicate a maximum stress (fig. 20) near 29 000 psi ( $20\,000\text{ N/cm}^2$ ).

The hot model support tube, when vibrated by itself, had a fundamental resonance frequency of about 30 hertz. This decrease in frequency from that of the cold model is due to the decrease in rigidity of the tube materials while hot (as simulated). The maximum stress shown in figure 20 is about 25 000 psi ( $17\,200\text{ N/cm}^2$ ), also a decrease from that of the cold model. Deflections and, consequently, strains are larger for the hot model but the stress is lower due to the much smaller modulus of elasticity in the hot portion of the tube. The hot-tube model was not tested within the aluminum tube without any springs as was done for the cold-tube model because of the expected large lateral deflections.

Presence of water and tube response. - The water surrounding the aluminum pressure tube affects the lateral bending response in three ways:

- (1) The motion of the tube through the water introduces viscous drag damping.
- (2) The water moving with the tube adds to the mass of the tube and tends to decrease the natural frequency and increase the displacement amplitude.
- (3) The water was vibrated in the fixture at the same g-level and in phase with the tube. Consequently, a pressure gradient was set up in the water which creates a buoyancy force on the aluminum pressure tube that tends to reduce displacement. This same condition would exist during boost phase of flight but might not be present during opera-

tion of the reactor. The effects of these pressure gradients were not included in the following calculations.

Water effects are demonstrated in the several test runs on the hot model and the aluminum pressure tube. The tests shown in figure 21(a) were made on only the pressure tube. Maximum stress near the center of the tube without water was 367 psi ( $253 \text{ N/cm}^2$ ), and the natural frequency was 167 hertz. When water was present around the aluminum tube, the stress value was 559 psi ( $385 \text{ N/cm}^2$ ), and the natural frequency was 43 hertz. The effect of the mass and viscosity of the water was calculated using the technique described in appendix B. The resulting virtual mass increase was calculated to be 32.6 pounds (14.79 kg), which is quite large compared with the 2.5 pounds (1.13 kg) for the pressure tube alone. Mass was then added to the dry tube in the form of copper collars clamped in a fairly uniform spacing along its length. A natural frequency of 42 hertz was observed in tests with 29.1 pounds (13.20 kg) added to the dry tube. This value agrees well with the value for the effect of mass only of the water (32.0 lb mass (14.50 kg)). During the test run with copper weights, the damping and buoyancy effects of the water were not present. A comparison of stress values for this run and the run in which these effects were present indicates that the buoyancy and damping reduced the stresses at the midpoint of the tube by a factor of approximately 6 (fig. 21(a)). The net result of the presence of water on the bending response of the pressure tube is still a large decrease in natural frequency and a significant increase in stress.

The effect of the water on the natural frequency of the pressure tube is just as large when the tube has two additional supports along its length. The dry tube had a natural frequency of 325 hertz compared with 80 hertz with water (fig. 21(b)).

In vibration tests of the entire fuel assembly, the mass of the water was a much smaller part of the total mass and its effect on natural frequency was small. The water caused a decrease in the natural frequency in all configurations tested including variations in the number of springs (from one to three) and in the number of lateral supports (from none to two). The effect of the water on stresses during these tests of the assembly was not as consistent. With no lateral supports on the pressure tube, the presence of water resulted in large reductions in peak stress with any number of springs (fig. 18), contrary to the pressure-tube-only results. Evidently in these cases, the damping and buoyancy forces due to the water were relatively more effective in reducing amplitudes than the virtual mass was in increasing amplitudes.

When the lateral supports were added to the pressure tube, the water had a very minor effect in reducing stress levels in the support tube. This is shown in figures 19(a) and (b) and 22. An apparent exception appears in the three-spring configuration, the stress distribution of which is plotted in figure 19(c). A comparison between tests with and without water in figure 19(c) should indicate the same effect of the water shown in figures 19(a) and (b). An examination of results from the tests without water in figures

19(b) and (c) suggests the possibility that the third spring was not tight in the latter test and was therefore ineffective. The test with water in figure 19(c) indicates that the third spring was working, perhaps having been tightened by the shrinkage of the pressure tube when the cool water was added around it.

Number of springs. - The springs placed in the annulus between the pressure tube and the support tube tend to join the two tubes and make their deflections the same. The extremes in the support-tube response (considering variations in number of springs only) are that of the two tubes moving entirely together and that of the tungsten tube moving by itself with no springs joining it to the pressure tube. The two tubes would move together if a large number of infinitely stiff springs joined them. The effect of the addition of any given spring depends on the existing relative deflections of the two tubes before the spring is added.

In tests on the cold vibration model, the addition of the first spring reduced the peak stress in the tungsten tube by more than a factor of 3 and increased the natural frequency from 41 to 53 hertz (figs. 20 and 17(a)). Adding the second and third springs within approximately 13 inches (33.0 cm) of the first had no significant effect on either stress level or natural frequency (figs. 17(b) and (c)). In other words, with the relative stiffness of the pressure tube and the tungsten support tube, the first spring added to connect the two tubes resulted in deflection curves so nearly the same that any additional springs did not further change the relative deflections.

Tests on the hot vibration model show anomalous behavior. The relative rigidity of the support tube with respect to the pressure tube is much less for the hot model than it was for the cold model. It is logical, therefore, that the additional springs might be more effective than they were for the case of the cold model. A second spring does, in fact, increase the natural frequency from 46 to 53 hertz. The third spring (fig. 18(c)), however, resulted in a decrease in natural frequency to a value even less than that observed with no spring. An examination of the stress curves for the pressure tube (fig. 18) indicates less reverse bending for the three-spring model and, consequently, the hot end support was not as fixed during the three-spring test as it was during the one- and two-spring tests. This would tend to account for the apparent discrepancies in behavior.

Amplitude of forcing function. - During the course of the testing, several tests were made in which the effect of varying the amplitude of the forcing function could be observed. For example, tests on the tube assembly as shown in figure 12(b) without water had input g-levels of 1.28 and 0.50 (an input ratio of 2.56); however, the stress ratio is less than 2. These results for the assembly without water indicate that the system damping was more effective at larger displacement (larger g-levels) than at the smaller displacement (smaller g-levels). It can be seen from the nonlinearity of the springs discussed in appendix C that this behavior could be expected. Large spring deflections on the order of a few mils result in a large hysteresis curve. An example of the order of

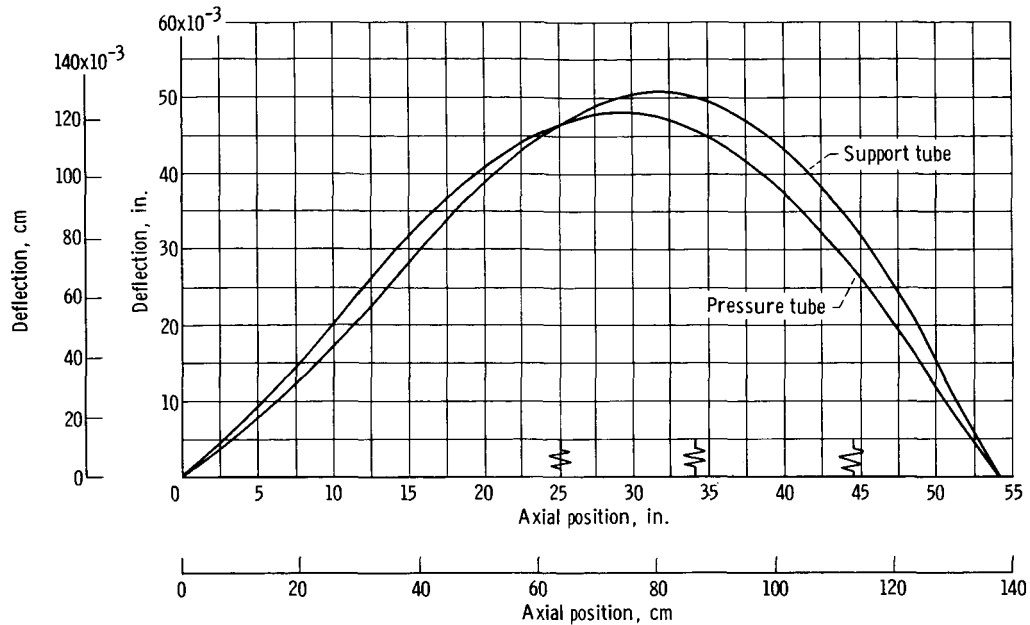


Figure 27. - Lateral deflection of tubes. No lateral supports; no water.

magnitude of the deflection curve for the model of figure 18(c) (three-spring model under 1.00-g lateral load) is shown in figure 27. The relative deflection between tubes is approximately 2 mils (0.05 mm), large enough to develop a considerable amount of damping. The deflection curve was obtained by the method outlined in appendix D using measured strains for the figure 18(c) dry test.

With water damping and buoyancy forces present (fig. 18(b)), the ratio of the stresses and the ratio of the input g-levels were more nearly equal, indicating that the damping effectiveness with water present was less dependent on the input g-level than when there was no water surrounding the tube.

The previously mentioned runs were made with no lateral supports to the pressure tube. A series of tests were made in which one support was used (figs. 23 and 24).

Prior to the start of these tests, new springs were installed. Two test runs were made in order to compare the behavior of the new springs with that with the first set of springs. These tests and the previous test are shown in figure 25. The natural frequency with the new springs was approximately 48 hertz compared with 44 hertz with the old springs. The difference may be due to differences among the sets of springs, tightness of the springs in the tubes, or fixity of the end support. The maximum stress levels were essentially the same in these three runs.

After these reference runs were made, the assembly was tested without water at g-levels from 0.58 to 3.50 (fig. 23). There was a large variation in natural frequency

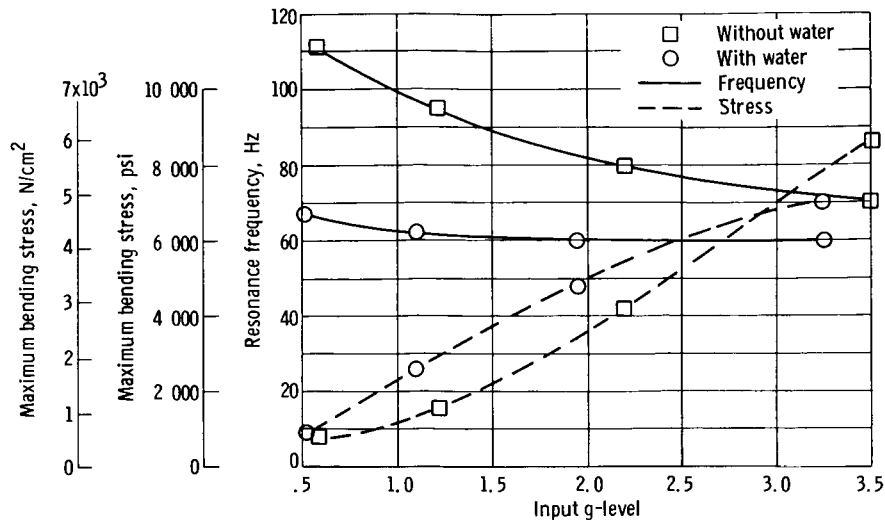


Figure 28. - Variation of frequency and maximum bending stress with input g-level.

over this range of inputs (see fig. 28) which may be the result of the nonlinearity of the spring constants of the corrugated springs as discussed in appendix C. It may also be that the natural frequency varies because the spring closest to the lateral support was slowly deforming as a result of the increasing g loads. A comparison of the stress distributions for the cases without water and those with water (figs. 23 and 24) indicates that the spring at the lateral support was becoming softer or loosening as the testing progressed. Upon disassembly it was noted that this spring was permanently distorted.

Pressure tube lateral support. - The rigidity of the pressure tube is greatly increased by the addition of the lateral support at midspan. Comparison of figures 18(a) and 22 indicates an increase in natural frequency from 38 to 52 hertz for the tube assembly with water and a single spring. The second lateral support near the entrance end has practically no effect on natural frequency and stress (figs. 19(a) and 22). It was decided therefore, that the second lateral support could be removed from the TWMR design.

For these cases with one corrugated spring, the peak stress in the pressure tube shows the same pattern of behavior as the natural frequency. Maximum stress is 1550 psi ( $1069 \text{ N/cm}^2$ ) with no support and drops to approximately 400 psi ( $276 \text{ N/cm}^2$ ) with either one or two additional supports.

This stiffening of the pressure tube does increase the effectiveness of adding springs between the tubes. With no lateral supports, a second spring increases the natural frequency 15 percent (figs. 18(a) and (b)) for the dry tubes. With two supports (figs. 19(a) and (b)), the second spring increases the natural frequency 53 percent.

## CONCLUSIONS

The TWMR fuel support assembly incorporates three springs in the annular space between tubes and a lateral support to the pressure tube at midspan. The two springs at the hot end are designed so that they are in contact with both the tungsten support tube and the aluminum pressure tube only after the support tube is hot. This prevents an excessive load on the tube and springs due to thermal expansion. Stresses at the resonant modes indicate that the assembly design is satisfactory from the standpoint of boost and flow-induced lateral bending vibrations.

The single-spring cold model that was tested did not have a midspan support during the test; however, the maximum stress was 8760 psi ( $6040 \text{ N/cm}^2$ ), a value less than the yield stress, and indicates satisfactory boost operation. Tests on a configuration designed to model the hot vibration characteristics of the assembly show that the support tube experiences stresses no higher than 1100 psi ( $760 \text{ N/cm}^2$ ) in regions where the expected yield strength is 3600 psi ( $2480 \text{ N/cm}^2$ ). This measured stress should be conservative because there is evidence that, in the test, the spring closest to the inlet end had loosened and lost some of its effectiveness. The TWMR support tube design is, therefore, considered feasible for assumed operating requirements.

Water surrounding the pressure tube has three separate effects on the behavior of the tube assembly; (1) virtual mass adds to the tube mass and, consequently, increases displacement amplitude, (2) viscous drag opposes displacement, and (3) the buoyancy decreases displacement amplitude. The overall effect of the water on stress was negligible for the support tube under boost conditions (i. e., under conditions with no lateral supports on the pressure tube). However, for conditions at the operating temperature, the stresses were decreased somewhat. In both cases, the natural frequencies were decreased slightly by the presence of the water.

The effect on the stress and frequency of addition of more than one corrugated spring to the cold support tube, which was tested without lateral supports, was very minor. It appears that the additional springs do, in general, decrease stresses in the hot support tube. Due to a complicated relation among the number of springs, the water, and the pressure tube lateral supports; however, a few exceptions to this generalization were observed. Three springs gave the lowest stress under the required design conditions.

The addition of lateral supports to the aluminum pressure tube greatly increases its rigidity, and, as such, reduces lateral displacements of the tungsten support tube when springs are installed to couple the tubes together. However, it was found that only one lateral support at midspan was necessary.

Lewis Research Center,  
National Aeronautics and Space Administration,  
Cleveland, Ohio, January 25, 1968,  
122-28-02-04-22.

## APPENDIX A

### MODEL DYNAMIC SIMILARITY

The two most important characteristics of the model for the support-tube prototype are the deflection curve and the natural frequency. These parameters should be identical for both model and prototype. The deflection curve may be found from

$$\frac{d^2y}{dx^2} = \frac{M_0}{EI} \quad (\text{A1})$$

where  $y$  is the lateral deflection,  $x$  is the position along tube axis,  $M_0$  is the bending moment, and  $EI$  is the flexural rigidity. (A more complete definition of the symbols is provided in appendix E.) It is assumed that the deflections are small and that the dynamic and static deflection curves differ only by some constant multiplication factor.

The model and prototype are essentially identical in overall size and mass distributions. Consequently, imposing the same boundary support conditions will result in identical deflection curves, providing that the model flexural rigidity ( $EI$ ) is equal to the prototype flexural rigidity along the entire tube length.

Flexural rigidity can easily be determined for the prototype as a function of axial position, and the model can be tailored to match this flexural rigidity (fig. 6) by varying the material and/or wall thickness of the support tube. The mass of the simulated fuel elements within the tube is much greater than the mass of the tube; as a result, a deviation in wall thickness will not result in any significant error because of the slight deviation in mass.

The natural frequency of a beam, found from energy methods as given in reference 7, is given by

$$\omega^2 = \frac{\int_0^l EI \left( \frac{d^2y}{dx^2} \right)^2 dx}{\int_0^l y^2 dm_x} \eta_1 \quad (\text{A2})$$

where  $m_x$  is the mass distribution along tube and  $l$  is the tube length. It has been shown that the deflection curves  $y(x)$  for the model and prototype will be the same because the flexural rigidity and the tube mass distribution for each tube are the same. These are the only variables that appear in the frequency equation (eq. A2)). Therefore,

the requirement of identical natural frequencies is satisfied.

The model must then satisfy the following requirements in order to obtain similarity in displacement and natural frequency:

$$(1) (EI)_m = (EI)_p$$

$$(2) (m_x)_m = (m_x)_p$$

$$(3) (\text{Boundary conditions})_m = (\text{Boundary conditions})_p$$

where the subscripts  $m$  and  $p$  are the model and prototype, respectively.

The stresses in the model and prototype will differ by ratio of the moduli of elasticity. Stress in the outermost fiber is given by

$$\sigma = \frac{M_0 a}{I} \quad (A3)$$

Substitution for the moment  $M_0$  from equation (A1) gives

$$\sigma = Ea \frac{d^2 y}{dx^2} \quad (A4)$$

Because the deflection curves are the same

$$\frac{\sigma_m}{\sigma_p} = \frac{(Ea)_m}{(Ea)_p} \quad (A5)$$

If  $a_m = a_p$  then

$$\sigma_p = \frac{E_p}{E_m} \sigma_m \quad (A6)$$

The measured strains can be multiplied by  $E_p$  to give the values of  $\sigma_p$  directly.

$$\sigma_p = E_p \epsilon_m \quad (A7)$$

## APPENDIX B

### DETERMINATION OF VIRTUAL MASS EFFECT OF WATER

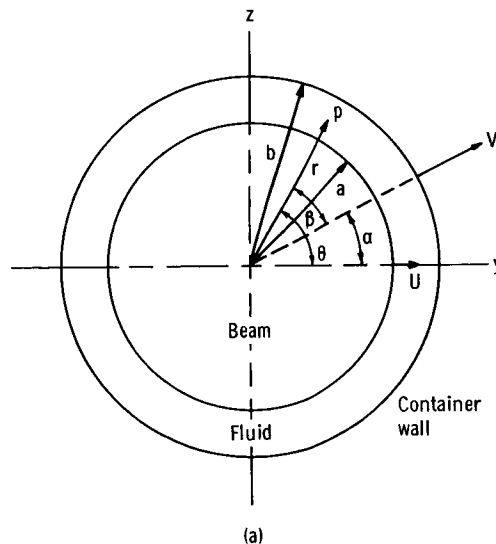
The presence of a fluid around the aluminum pressure tube will have three known effects: (a) viscous damping, (b) virtual mass increase, and (c) buoyancy. The buoyancy effects were neglected in the calculations.

For an inviscid fluid and for a very large container in comparison with the dimensions of the beam, the virtual mass increase is equal to the mass of the fluid displaced by the beam (ref. 8). This virtual mass increase is an effective drift mass of the fluid which has been displaced because of the flow movement around the cylinder. The virtual mass increase is given by

$$m' = \pi a^2 \rho l \quad (\text{B1})$$

where  $m'$  represents an increase in effective mass of a cylinder of mass  $m$  as it moves through a fluid of density  $\rho$ . Corrections are required for viscous fluids and for container walls near the beam.

The correction for the nearness of the container wall can be derived by a technique similar to that given in reference 8 for concentric spheres using velocity potentials. The parameters used in the derivation are shown in sketch (a).



For fluid motion that is irrotational, a scalar potential exists such that

$$\frac{\partial \phi}{\partial s} = V_s \quad (\text{B2})$$

$$\vec{V} = \text{grad } \phi \quad (\text{B3})$$

Impulses are supplied to the cylinder and container to create motions  $U$  and  $V$ , respectively. Motions are assumed to be steady state and at the initial instant that the centers coincide. Boundary conditions are

$$\frac{\partial \phi}{\partial r} = -U \cos \theta \quad \text{at surface a} \quad (\text{B4})$$

$$\frac{\partial \phi}{\partial r} = -V \cos \beta \quad \text{at surface b} \quad (\text{B5})$$

A unit vector in the direction of point  $p$  is

$$\vec{i} \cos \theta + \vec{j} \sin \theta$$

and a unit vector along the direction of velocity  $V$  is

$$\vec{i} \cos \alpha + \vec{j} \sin \alpha$$

The scalar product of these vectors is

$$\cos \beta = \cos \theta \cos \alpha + \sin \theta \sin \alpha \quad (\text{B6})$$

Because

$$y = r \cos \theta$$

$$z = r \sin \theta$$

then

$$\cos \beta = \frac{y}{r} \cos \alpha + \frac{z}{r} \sin \alpha$$

The potential  $\varphi$  is the result of rectilinear flow with doublets, both of unknown strength. The relation for  $\cos \beta$  and the boundary conditions suggest  $\varphi$  of the form

$$\varphi = A_1 r \cos \theta + B_1 \frac{\cos \theta}{r} + A_2 r \sin \theta + B_2 \frac{\sin \theta}{r} \quad (\text{B8})$$

and

$$\frac{\partial \varphi}{\partial r} = A_1 \cos \theta - B_1 \frac{\cos \theta}{r^2} + A_2 \sin \theta - B_2 \frac{\sin \theta}{r^2} \quad (\text{B9})$$

Evaluating at the boundary gives

$$\left( A_1 - \frac{B_1}{a^2} \right) \cos \theta + \left( A_2 - \frac{B_2}{a^2} \right) \sin \theta = -U \cos \theta \quad (\text{B10})$$

$$\left( A_1 - \frac{B_1}{b^2} \right) \cos \theta + \left( A_2 - \frac{B_2}{b^2} \right) \sin \theta = -V \cos \beta \quad (\text{B11})$$

These equations must hold at any  $\theta$  on boundary a and b. Consequently, the right and left sides of the equations are identically satisfied. Therefore, the coefficients must be equal, or

$$A_1 - \frac{B_1}{a^2} = -U \quad (\text{B12})$$

$$A_2 - \frac{B_2}{a^2} = 0 \quad (\text{B13})$$

and from the second equation and equation (B6)

$$A_1 - \frac{B_1}{b^2} = -V \cos \alpha \quad (\text{B14})$$

$$A_2 - \frac{B_2}{b^2} = -V \sin \alpha \quad (\text{B15})$$

Solving for the constants gives

$$A_1 = \frac{1}{b^2 - a^2} (Ua^2 - b^2V \cos \alpha) \quad (\text{B16})$$

$$B_1 = \frac{a^2b^2}{b^2 - a^2} (U - V \cos \alpha) \quad (\text{B17})$$

$$A_2 = -\frac{b^2}{b^2 - a^2} V \sin \alpha \quad (\text{B18})$$

$$B_2 = -\frac{a^2b^2}{b^2 - a^2} V \sin \alpha \quad (\text{B19})$$

which defines the potential for concentric cylinders at the instant that the boundaries are concentric. Finally, the potential must satisfy Laplace's equation

$$\frac{\partial}{\partial r} \left( r \frac{\partial \varphi}{\partial r} \right) + \frac{1}{r} \frac{\partial^2 \varphi}{\partial \theta^2} = 0 \quad (\text{B20})$$

Taking the derivatives

$$\frac{\partial}{\partial r} \left( r \frac{\partial \varphi}{\partial r} \right) = \left( A_1 + \frac{B_1}{r^2} \right) \cos \theta + \left( A_2 + \frac{B_2}{r^2} \right) \sin \theta \quad (\text{B21})$$

and

$$\frac{1}{r} \frac{\partial^2 \varphi}{\partial \theta^2} = -\left( A_1 + \frac{B_1}{r^2} \right) \cos \theta - \left( A_2 + \frac{B_2}{r^2} \right) \sin \theta \quad (\text{B22})$$

Therefore, Laplace's equation is satisfied.

Now, if  $\alpha = 0$ , which is the case in these tests,

$$\varphi = \left[ \frac{r}{b^2 - a^2} (Ua^2 - Vb^2) + \frac{a^2 b^2}{b^2 - a^2} \frac{1}{r} (U - V) \right] \cos \theta \quad (\text{B23})$$

The impulsive pressure on a surface with potential  $\varphi$  is defined as

$$\tilde{\omega} = \rho \varphi \eta_2 \quad (\text{B24})$$

On surface a

$$\tilde{\omega}_a = \rho \varphi_a \eta_2 \quad (\text{B25})$$

and on surface b

$$\tilde{\omega}_b = \rho \varphi_b \eta_2 \quad (\text{B26})$$

or

$$\tilde{\omega}_a = \rho \cos \theta \left[ \frac{Ua}{b^2 - a^2} (a^2 + b^2) - \frac{2Vab^2}{b^2 - a^2} \right] \eta_2 \quad (\text{B27})$$

$$\tilde{\omega}_b = \rho \cos \theta \left[ \frac{2Ua^2 b}{b^2 - a^2} - \frac{Vb}{b^2 - a^2} (b^2 + a^2) \right] \eta_2 \quad (\text{B28})$$

The impulsive pressures can be integrated to obtain an impulsive force of the liquid on the boundaries in the direction of motion. Impulsive force on the beam (surface a) is

$$\begin{aligned} \mathcal{F}_a &= 2 \int_0^\pi \tilde{\omega}_a \cos \theta l a \, d\theta \\ &= l \pi a \rho \left[ \frac{Ua}{b^2 - a^2} (a^2 + b^2) - \frac{2Vab^2}{b^2 - a^2} \right] \end{aligned} \quad (\text{B29})$$

and the impulsive force on the outer surface (container wall) is

$$\begin{aligned} \mathcal{J}'_b &= 2 \int_0^\pi \tilde{\omega}_b \cos \theta \, l b \, d\theta \\ &= l \pi b \rho \left[ \frac{2U a^2 b}{b^2 - a^2} - \frac{V b}{b^2 - a^2} (b^2 + a^2) \right] \end{aligned} \quad (\text{B30})$$

The impulsive force of the boundary on the fluid is the negative of equations (B29) and (B30).

$$\mathcal{J}'_a = - \mathcal{J}_a \quad (\text{B31})$$

$$\mathcal{J}'_b = - \mathcal{J}_b \quad (\text{B32})$$

The difference in impulses is equal to the change in momentum of the fluid

$$\begin{aligned} \mathcal{J}'_a - \mathcal{J}'_b &= \pi \rho a^2 l U - \pi \rho b^2 l V \\ &= m'_a U - m'_b V \end{aligned} \quad (\text{B33})$$

where  $m'_a$  represents the mass of fluid displaced by the inner cylinder, and  $m'_b$  represents the mass within the container if filled with a fluid of density  $\rho$ . The difference between the impulse to start the inner cylinder motion, defined as  $J$ , and the impulse of fluid on the inner cylinder,  $\mathcal{J}_a$ , will represent the momentum of the cylinder itself, or

$$J - \mathcal{J}_a = mU \quad (\text{B34})$$

If the motion of the container  $V = 0$  (only relative motion  $U$  considered), then

$$\mathcal{J}_a = \pi \rho a^2 l U \left( \frac{a^2 + b^2}{b^2 - a^2} \right) \quad (\text{B35})$$

Substituting equation (B35) into equation (B34) gives

$$\begin{aligned}
J &= mU + \pi\rho a^2 \ell U \left( \frac{a^2 + b^2}{b^2 - a^2} \right) \\
&= \left[ m + m' \left( \frac{a^2 + b^2}{b^2 - a^2} \right) \right] U
\end{aligned} \tag{B36}$$

The virtual mass increase of the cylinder, including the effect of the nearness of the container wall, is then

$$m' \left( \frac{a^2 + b^2}{b^2 - a^2} \right) \tag{B37}$$

Note that, as  $b$  becomes very large compared with  $a$ , the corrective term goes to 1 and the virtual mass increase approaches  $m'$ .

The correction for viscosity on the virtual mass increase may be found from references 9 and 10. The correction, involving the fluid viscosity, period of oscillation, and size of the cylinder, is in the form (where higher order terms are neglected)

$$\left( 1 + \frac{2\lambda}{a} \right) \tag{B38}$$

where  $\lambda = (\mu\tau/\pi\rho)^{1/2}$  is the penetration depth,  $\tau$  is the period of oscillation,  $\mu$  is the absolute viscosity,  $\rho$  is the fluid density, and  $a$  is the cylinder radius. The virtual mass increase

$$m' \left( \frac{a^2 + b^2}{b^2 - a^2} \right)$$

is replaced by

$$m' \left( 1 + \frac{2\lambda}{a} \right) \left( \frac{a^2 + b^2}{b^2 - a^2} \right)$$

An overall correction term for viscosity and wall effects may now be defined as

$$k_0 = \left(1 + \frac{2\lambda}{a}\right) \left(\frac{a^2 + b^2}{b^2 - a^2}\right)$$

Therefore, the virtual mass becomes

$$M = m + k_0 m'$$

Evaluating the penetration depth  $\lambda$  for a frequency of 40 hertz and for water yields

$$\lambda = 1.19 \times 10^{-2} \text{ in. (or } 3.02 \times 10^{-2} \text{ cm)}$$

so that the viscosity correction is 1.02. Similarly, the wall correction may be determined. Because the container used in the test had a square cross section, the radius  $b$  must be evaluated between the limits of 1.5 and 2.12 inches (3.81 and 5.38 cm), the distance to the center and corner, respectively. For a tube radius of 1.25 inches (3.18 cm), the correction factor varies from 5.53 to 2.07, depending on the equivalent container radius. If the container is equated to a cylinder with the same cross-sectional area, the correction for the wall effect is 3.4. The mass of the displaced water  $m'$  is 9.4 pounds mass (4.26 kg) and the virtual mass increase, including both the viscosity and wall effect, is 32.6 pounds mass (14.79 kg). Considering wall effect alone, the calculated virtual mass increase due to water is 32.0 pounds mass (14.50 kg).

The virtual mass directly affects the natural frequency of a beam. Consequently, an expression relating the mass and frequency, such as given in reference 11, can be used to estimate the virtual mass from the natural frequency of the tube in water. This method depends on exactly evaluating end conditions. Applying the expression to the test of the aluminum pressure tube, results in an approximate virtual mass increase of 26.3 pounds mass (11.93 kg).

With this as a starting point, a number of copper weights of approximately 1.26 pounds mass (574 g) each were distributed along the tube to simulate the mass of the water. The number of weights were varied until the natural frequency of the dry tube with weights matched that of the wet tube. This occurred when 29.1 pounds mass (13.20 kg) were added to the tube and shows good agreement with the corresponding calculated value, neglecting viscosity and buoyancy effects, of 32.0 pounds mass (14.50 kg). This agreement indicates that buoyancy did not have a large effect on the natural frequency of the pressure tube surrounded by water.

## APPENDIX C

### CORRUGATED SPRING CHARACTERISTICS

Tests were performed to determine the characteristics of the corrugated spring used in the TWMR fuel-support design.

To determine the spring constant, corrugated tungsten springs 1.00-inch (2.54-cm) wide by 0.005-inch (0.013-cm) thick were held between two aluminum cylinders whose spring contact dimensions were the same as the TWMR pressure tube and support tube. The loading was applied with a yoke on the inner cylinder such that uniform loading across the width of the spring would occur. Deflections were read directly on two dial indicators, which read in increments of 0.001 inch (0.0025 mm). Loads were applied in 5-pound-force (22.2-N) increments.

Four different springs were tested: each had a different degree of tightness between the cylinders representing variations in manufacturing tolerances. The static load deflection curves are shown on figure 29. The tighter the fit, the higher the initial loading required to initiate a measurable deflection. A loose fit appears to require no initial load. For example, a 0.002-inch (0.005-cm) loose fit started to deflect immediately on load application. The preload is required for a tight fit because the spring is compressed at each lobe and to initiate deflection requires an initial loading to overcome friction. The spring lobes initially act as columns requiring a high loading for a small deflection. As the spring flattens under load it acts as a cantilever spring and the spring rate changes to

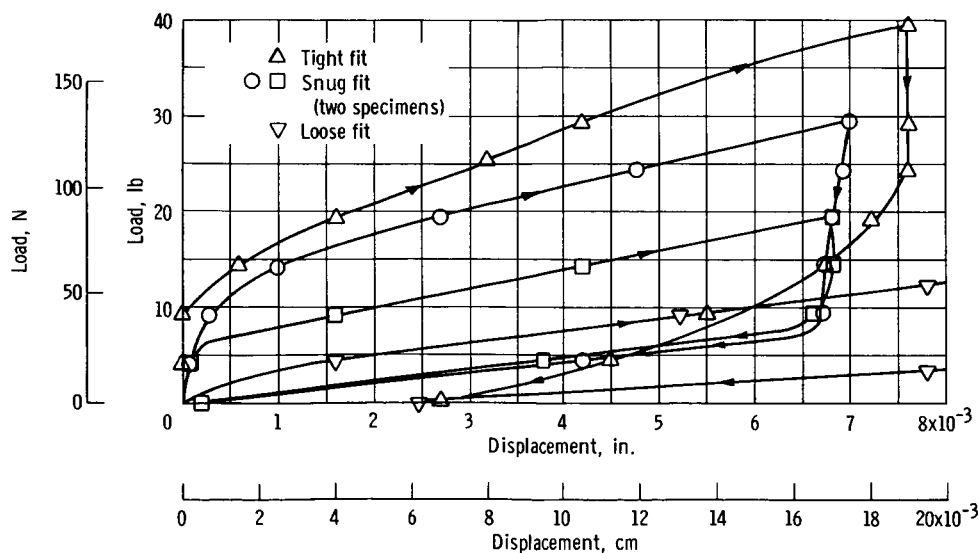


Figure 29. - Load-displacement characteristics of 1.00-inch (2.54-cm) wide by 0.005-inch (0.013-cm) thick 11-lobe corrugated tungsten spring.

a lower value. All the springs had parallel constant slopes but were displaced by the initial friction preload.

When the load was reduced, contact friction caused displacement lags, resulting in a hysteresis curve. All the spring unloading curves were approximately the same once the initial preload was removed.

The initial spring rate was an average of 50 000 pounds per inch (87 600 N/cm) dropping off to a standing spring rate of approximately 3000 pounds per inch (5250 N/cm).

The tighter fits caused greater hysteresis losses and therefore have greater damping in a vibration environment. Not only does the fit affect the spring constant, but also a tight fit may result in permanent deformations in the spring lobes. This indicates that the specification of a manufacturing tolerance is quite important for this application.

## APPENDIX D

### DEFLECTION CURVE CALCULATIONS

The deflection curve for the support tube and aluminum pressure tube can be calculated from the stress-strain relations for bending of beams (ref. 12). The strains obtained experimentally from the strain gages are related to the radius of curvature of the beam by

$$\frac{1}{R} = -\frac{\epsilon}{a} \quad (D1)$$

where  $R$  is the radius of curvature,  $\epsilon$  is the strain at the surface of the tube, and  $a$  is the radius from neutral axis to tube surface. The radius of curvature is also related to the deflection by the relation

$$\frac{d^2y}{dx^2} = \frac{1}{R} \quad (D2)$$

where  $y$  is the deflection and  $x$  is the axial position. The deflection can be found from integration of equation (D2)

$$y = \int_0^x \left( \int_0^x \frac{1}{R} dx \right) dx \quad (D3)$$

The integration can be accomplished numerically if a sufficient number of values of the radius of curvature are known along the length of the beam. The equation reduces to

$$y_k = \sum_{j=0}^k \left( \sum_{i=0}^j \frac{1}{R_i} \Delta x_i + C_1 \right) \Delta x_j + C_2 \quad (D4)$$

where the constant  $C_2$  determines the rigid body translation of the tube neutral axis and  $C_1$  determines the rigid body rotation of the neutral axis. For purposes of comparing relative deflections along the beam,  $C_2$  can be set to zero, and  $C_1$  found from a con-

stant slope resulting from the differences between deflections of the ends of the beam.

Good accuracy can only be obtained if the number of points for which the radius of curvature is known is high. There are enough variations in materials, diameters, etc., along the tungsten tube and aluminum tube that 10 gage locations are not sufficient, especially at the inlet end, to accurately determine its radius of curvature. Differences in assumed radius of curvature are apparent in the deflection curves of figure 27 in the apparent crossover point of the tubes at approximately midspan. Because an annular gap does exist between the tubes, such behavior is possible. However, the relative displacement between tubes should be taken only as approximate.

## APPENDIX E

### SYMBOLS

$A_{1,2}$	strength of rectilinear flow potentials, in./sec; cm/sec	$k_0$	virtual mass correction factor for both viscosity and nearness of container wall
$a$	radius from tube axis to outer surface, in.; cm	$l$	tube length, in.; cm
$B_{1,2}$	strength of flow doublet potentials, in. <sup>3</sup> /sec; cm <sup>3</sup> /sec	$M$	virtual mass, lb mass; kg
$b$	inside radius of container, in.; cm	$M_0$	bending moment, (in.)(lb); (cm)(N)
$C_1$	constant of integration representing rigid body rotation of tube neutral axis, radians	$m$	tube mass, lb mass; kg
$C_2$	constant of integration representing rigid body translation of tube neutral axis, in.; cm	$m_x$	mass distribution along tube, slug; kg
$E$	modulus of elasticity, psi; N/cm <sup>2</sup>	$m'$	mass of displaced water, lb mass; kg
$EI$	flexural rigidity, (lb)(in. <sup>2</sup> ); (N)(cm <sup>2</sup> )	$R$	radius of curvature of deflected tube, in.; cm
$f_n$	natural frequency, Hz	$r$	radius to any point within the fluid between the tube surface and container wall, in.; cm
$I$	moment of inertia, in. <sup>4</sup> ; cm <sup>4</sup>	$s$	general direction coordinate for velocity potential
$\mathcal{J}$	impulsive force of fluid on boundaries, (lb)(sec); (N)(sec)	$U$	lateral velocity of tube, in./sec; cm/sec
$\mathcal{J}'$	impulsive force of boundaries on fluid, (lb)(sec); (N)(sec)	$V$	lateral velocity of container, in./sec; cm/sec
$\vec{i}$	unit vector in direction $y$	$V_s$	velocity in direction $s$ derived from the first derivative of the velocity potential, in./sec; cm/sec
$J$	impulsive force required to start tube into motion, (lb)(sec); (N)(sec)	$\vec{V}$	velocity vector of fluid
$\vec{j}$	unit vector in direction $z$		

x	position along axis of tube, in.; cm	$\mu$	absolute viscosity of fluid, lb mass/(sec)(in.); kg/(sec)(cm)
y	lateral displacement of tube, position coordinate, in.; cm	$\rho$	density of fluid, lb mass/in. <sup>3</sup> ; kg/cm <sup>3</sup>
z	position perpendicular to direc- tion of motion of tube, in.; cm	$\sigma$	stress, psi; N/cm <sup>2</sup>
$\alpha$	angle between relative motion of tube and container, radians	$\tau$	period of oscillation, sec
$\beta$	angle from direction of motion of container to some point in the fluid, radians	$\varphi$	velocity potential, in. <sup>2</sup> /sec; cm <sup>2</sup> /sec
$\epsilon$	strain, in./in.; cm/cm	$\omega$	angular frequency, rad/sec
$\eta_1$	unit conversion factor, 12 in./ft; 100 cm/m	$\tilde{\omega}$	local impulsive pressure, (psi)(sec); (N/cm <sup>2</sup> )(sec)
$\eta_2$	unit conversion factor, $\frac{1}{386} \frac{(\text{lb force})(\text{sec}^2)}{(\text{lb mass})(\text{in.})}, \frac{1}{100} \frac{(\text{N})(\text{sec}^2)}{(\text{kg})(\text{cm})}$	Subscripts:	
$\theta$	angle from direction of motion of tube to some point in the fluid, radians	a	tube outer surface
$\lambda$	penetration depth, in.; cm	b	container inner surface
		i	i <sup>th</sup> location
		j	j <sup>th</sup> location
		k	k <sup>th</sup> location
		m	model
		p	prototype

## REFERENCES

1. Krasner, M. H.: Feasibility Study of a Tungsten Water-Moderated Nuclear Rocket. V. Engine System. NASA TM X-1424, 1968.
2. Aase, D. T.; Kempf, F. J.; O'Keefe, D. P.; Townsend, W. C.; and Trent, D. S.: Tungsten Water-Moderated Reactor Fuel Support Design Analysis. Battelle-Northwest (NASA CR-72031), Aug. 1966.
3. Cox, T. H.; Gjertsen, R. K.; Guenther, E., Jr.; Kaufman, S.; Schumann, F. A.; and Trushin, J. T.: Fuel Assembly Design Study for the Tungsten Water-Moderated Reactor (TWMR). Rep. No. MND-3271 (NASA CR-72024). Martin Co., Aug. 31, 1966.
4. Schmidt, F. F.; and Ogden, H. R.: The Engineering Properties of Tungsten and Tungsten Alloys. DMIC Rep. 191, Battelle Memorial Inst., Sept. 27, 1963. (Available from DDC as AD-425547.)
5. Weiss, V.; and Sessler, J. G., eds: Ferrous Alloys. Vol. 1 of Aerospace Structural Metals Handbook. Third rev., Syracuse University Press, Mar. 1966.
6. Wilson, J. W.; and Tietz, T. E.: Behavior and Properties of Refractory Metals. Stanford University Press, 1965.
7. Thompson, William T.: Mechanical Vibrations. Second ed., Prentice-Hall, Inc., 1953.
8. Milne-Thomson, Louis M.: Theoretical Hydrodynamics. Third ed., Macmillan Company, 1955.
9. Stokes, G. G.: On the Effects of the Internal Friction of Fluids on the Motion of Pendulums. Cambridge Philo. Soc. Trans., vol. 9, 1850, pp. 8-106.
10. Hussey, R. G.; and Vujacic, Peter: Damping Correction for Oscillating Cylinder and Sphere. Phys. Fluids, vol. 10, no. 1, Jan. 1967, pp. 96-97.
11. Harris, Cyril M.; and Crede, Charles E., eds: Shock and Vibration Handbook. Vol. 1. McGraw-Hill Book Co., Inc., 1961.
12. Crandall, Stephen H.; and Dahl, Norman C., eds: An Introduction to the Mechanics of Solids. McGraw-Hill Book Co., Inc., 1959.
13. Weiss, V.; and Sessler, J. G., eds: Nonferrous Light Metal Alloys. Vol. II of Aerospace Structural Metals Handbook. Third rev., Syracuse University Press, Mar. 1966.